Agricultural and Forest Meteorology 366 (2025) 110465

Contents lists available at ScienceDirect

Agricultural and Forest Meteorology

journal homepage: www.elsevier.com/locate/agrformet

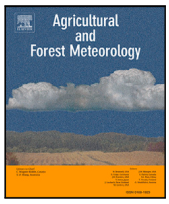

Lower carbon uptake rates resulting from converting wooded Cerrado to pasture-dominated agricultural area in the Brazilian savanna

Yuqing Zhao [a], David Holl [a,*], Jamil A.A. Anache [b], Alex N.A. Kobayashi [b,c], Edson Wendland [b]

[a] Institute of Soil Science, Center for Earth System Research and Sustainability (CEN), Universität Hamburg, Allende-Platz 2, Hamburg, 20146, Germany
[b] São Carlos School of Engineering, University of São Paulo (EESC-USP), Avenida Trabalhador São-carlense, 400, São Carlos, SP, 13566-590, Brazil
[c] The Centre for Hydrogeology and Geothermics, University of Neuchâtel (CHYN-UNINE), Rue Emile-Argand 11, Neuchâtel, 2000, Switzerland

ARTICLE INFO

Dataset link: https://ameriflux.lbl.gov/sites/siteinfo/BR-IAB, https://doi.org/10.5281/zenodo.13912437, https://doi.org/10.5281/zenodo.12528643, https://doi.org/10.5281/zenodo.11123751

Keywords:
Woodland
Cultivated pasture
Carbon flux
Land use change
NEE partitioning

ABSTRACT

Agricultural expansion in the Brazilian Cerrado ecoregion has been causing extensive land use and land cover changes (LULCC), drastically shifting the carbon cycle dynamics of the affected ecosystems. However, accurate in situ observations of the net ecosystem exchange of carbon dioxide (NEE) from wooded Cerrado (*Cerrado sensu stricto*) as well as from post-conversion agricultural landscapes are lacking, with the limited amount of impact assessments in the literature being primarily based on remotely sensed data. This study presents a multi-annual time series of temporal high-resolution eddy covariance carbon dioxide fluxes, measured on the border between a wooded Cerrado and a post-conversion agricultural area, primarily used as a pasture, in southeastern Brazil. We investigated multiple setups of NEE partitioning methods to separate NEE into its components gross primary production (GPP) and total ecosystem respiration (TER). We combined these component partitioning models with source area partitioning methods to estimate component fluxes for the two contrasting ecosystems within the tower footprint. Model results were compared against remotely sensed vegetation indices and flux data from similar ecosystems. We found that converting native wooded Cerrado to a pasture-dominated agricultural area decreased the landscape's NEE carbon (NEE-C) uptake by up to 494 g m^{-2} yr^{-1} (73 %). The wooded Cerrado had an annual cumulative NEE-C of -639 ± 20 g m^{-2} yr^{-1} and -673 ± 19 g m^{-2} yr^{-1} in 2019 and 2020, respectively. In comparison, the pasture had lower annual cumulative NEE-C of -146 ± 39 g m^{-2} yr^{-1} and -179 ± 38 g m^{-2} yr^{-1} in the same years. The pasture exhibited lower light use efficiency (LUE) and NEE-C uptake in the dry season, resulting in lower annual NEE-C uptake. Additionally, the pasture showed greater sensitivity to precipitation changes, leading to higher seasonal variations in carbon dioxide fluxes.

1. Introduction

The Brazilian Cerrado is a tropical savanna ecoregion featuring various ecosystem types including woodlands, savannas, grasslands, dry forests, and gallery forests (Klink and Machado, 2005). Depending on the physiognomy of the landscape, Cerrado is further categorized into *campo sujo*, *campo Cerrado*, *Cerrado sensu stricto*, and *cerradão*, each having a higher canopy cover percentage compared to the previous one (Goodland, 1971). As the second largest biome of Brazil, Cerrado covers 21% of the country and is home to more than 160,000 plant, fungi, and animal species (Klink and Machado, 2005; Ratter et al., 1997). However, the Brazilian Cerrado has been experiencing rapid land use and land cover changes (LULCC) due to agricultural expansion, leading to changes in carbon dioxide (CO_2) fluxes between these ecosystems and the atmosphere (Batlle-Bayer et al., 2010; Cunha et al., 2015). The agricultural expansion in the Cerrado started in the mid-1950s and was boosted by government policies, which facilitated the land use conversion rate significantly (Silva et al., 2006). Agricultural development in the region was long limited by the lack of infrastructure and poor soil quality (Silva et al., 2006). Specifically, the soils in the Brazilian Cerrado are dominated by highly weathered Oxisols with low fertility and low pH, which are unsuitable for agricultural purposes (Santana and Bahia Filho, 1998; Hartemink et al., 2020). Since the 1970s, the application of modern agricultural technologies, including plant breeding, soil conditioning, and soil management, has improved soil fertility, making them more suitable for crop production (Santana and Bahia Filho, 1998). In addition, the construction of

* Corresponding author.
E-mail address: david.holl@uni-hamburg.de (D. Holl).

https://doi.org/10.1016/j.agrformet.2025.110465
Received 2 July 2024; Received in revised form 11 February 2025; Accepted 18 February 2025
Available online 11 March 2025

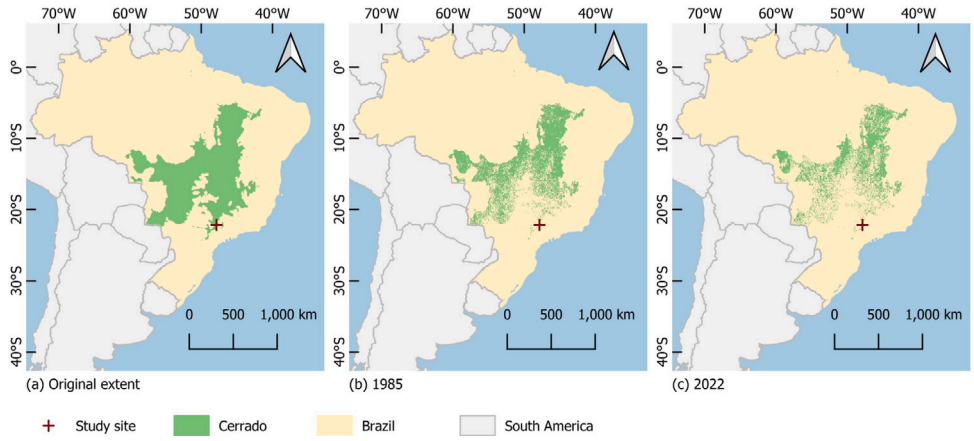

Fig. 1. The changes in the extent of Cerrado due to LULCC. *Source:* Adapted from MapBiomas database (Souza et al., 2020) and (Olson et al., 2001).

the new capital, Brasilia, in the Brazilian Cerrado ecoregion facilitated the development of infrastructure, improving the transportation of agricultural products (Silva et al., 2006). Since then, LULCC in the Brazilian Cerrado has been extensive. The annual land use conversion rate peaked in the early 1970s at about 40,000 km^2 yr^{-1} (Klink and Machado, 2005). The conversion remained at a high rate until the mid-2000s, ranging from 22,000 to 30,000 km^2 yr^{-1}, which was higher than the annual deforestation rate in the Amazon (Machado et al., 2004; Klink and Machado, 2005). By 2005, more than 50 % of the Brazilian Cerrado had been converted to pasture and agricultural land (Klink and Machado, 2005). Recent land use assessments made by MapBiomas platform (Souza et al., 2020) estimated that in 2022, 45 % of the natural Cerrado land cover remains (forested and open fields areas), and it decreased 27 % between 1985 and 2022 (Fig. 1).

Among the different types of LULCC, the conversion of native Cerrado into pastures, predominantly for cattle grazing, is one of the major types (Carvalho et al., 2010; Sanchez, 1979). This management practice replaces native Cerrado vegetation with cultivated grasses, resulting in changes in CO_2 fluxes between these landscapes and the atmosphere (Carvalho et al., 2010). National land policies facilitated this type of land use conversion in the 1970s (Batista and Norat, 2019). By 1977, the Program for the Development of the Cerrado (POLOCENTRO) had financed 8,000 km^2 of land for agricultural use (Sanchez, 1979). Of the land funded by the program, 4,000 km^2 (50%) were directly converted to cultivated pastures (Sanchez, 1979). An additional 3,200 km^2 (40%) were initially converted to cropland for rice production for the first one to three years, after which they were also converted into cultivated pastures (Sanchez, 1979). As a result, by the year 2005, planted pastures had occupied around 42% of the core area of the Cerrado (Klink and Machado, 2005), which raises the question of how this type of conversion would affect the CO_2 flux of the land.

Accurate measurement of the net ecosystem exchange (NEE) of CO_2 for both native Cerrado and planted pasture under the same meteorological conditions is therefore necessary. Eddy covariance (EC) studies on the carbon fluxes of native Cerrado are scarce and results vary due to the complexity of the different ecosystems subsumed in the Cerrado ecoregion with its diverse tree physiognomies and climate conditions (Alves et al., 2021; Vourlitis et al., 2022). For example, da Rocha et al. (2002) and Miranda et al. (1997) estimated the wooded Cerrado (*Cerrado sensu stricto*), the most dominant form of Cerrado (Carvalho et al., 2008), to be a weak sink of CO_2, with strong seasonal variability. The strong net CO_2 uptake in the wet season is balanced by net CO_2 emission in the dry season, resulting in an overall balanced, sometimes negative, annual NEE (da Rocha et al., 2002). On the other hand, Vourlitis and da Rocha (2010) reported that the Cerrado transitional forest (*cerradão*) is a small source of carbon, with an annual average daily NEE of CO_2-C (NEE-C) around 0.19 ± 0.24 g m^{-2} d^{-1} (Vourlitis and da Rocha, 2010). For a seasonally flooded Cerrado forest (*mata de galeria*) in the Pantanal ecoregion close to the border of the Cerrado ecoregion, Vourlitis et al. (2022) reported average NEE-C uptake values derived from multi-annual EC measurements observed and reported by Dalmagro et al. (2019) of 230 g m^{-2} yr^{-1}. The interannual variability of this wetland gallery forest was large with it changing from a NEE-C source to a sink in both years reported in Vourlitis et al. (2022). The latter authors could verify the EC carbon budgets with inventory methods.

Santos et al. (2003) found that a grass-dominated Cerrado woodland (*campo sujo*) acted as a strong carbon sink, achieving an annual NEE-C uptake of $-456\,g\,m^{-2}\,yr^{-1}$. However, Arruda et al. (2016) suggested *campo sujo* could become a carbon source under drought conditions with a NEE-C release of $357\,g\,m^{-2}\,yr^{-1}$. In summary, the limited studies on native Cerrado's carbon uptake conducted in the early 2000s yielded varying results. Due to the small sample size, these studies may not accurately reflect the magnitude and seasonality of each Cerrado subcategory. In contrast, planted pastures in the Cerrado are widely recognized as strong carbon sinks, with a NEE-C around $-200\,g\,m^{-2}\,yr^{-1}$ (Alves et al., 2021; Bezerra et al., 2022; Roberti et al., 2024). These pastures typically exhibit a higher carbon assimilation rate than the native Cerrado, but they are more sensitive to variations in precipitation and soil fertility (Alves et al., 2021; Santos et al., 2004; Miranda et al., 1997). However, existing studies lack a direct comparison of the carbon uptake of pastures and native Cerrado in the same area under identical meteorological conditions.

In this study, we aim to estimate the impact of converting a wooded Cerrado into a pasture-dominated agricultural area on the CO_2 flux dynamics of such a landscape by using EC-measured NEE fluxes. We present a multi-annual time series of temporal high-resolution EC CO_2 fluxes, measured on the border between a wooded Cerrado and a post-conversion agricultural area, which was primarily used as a pasture, in Itirapina, Brazil. We recognize certain methodological challenges, specifically the partitioning of the measured net CO_2 fluxes into component fluxes of opposing directions, which are related to different ecosystem processes, namely total ecosystem respiration (TER) and gross primary production (GPP). In order to account for plant development in the course of a vegetation period, subsets of data have been used in the literature (e.g. (Holl et al., 2019a)) to fit combined temperature and light response models to estimate model parameter time series, which can then be interpreted as the seasonal course of ecosystem functional properties (EFP). The temporal resolution of these model parameter time series should be appropriate to partition the dataset at hand (i.e. using enough data to obtain robust parameter estimates per time step while using enough subsets of data to properly

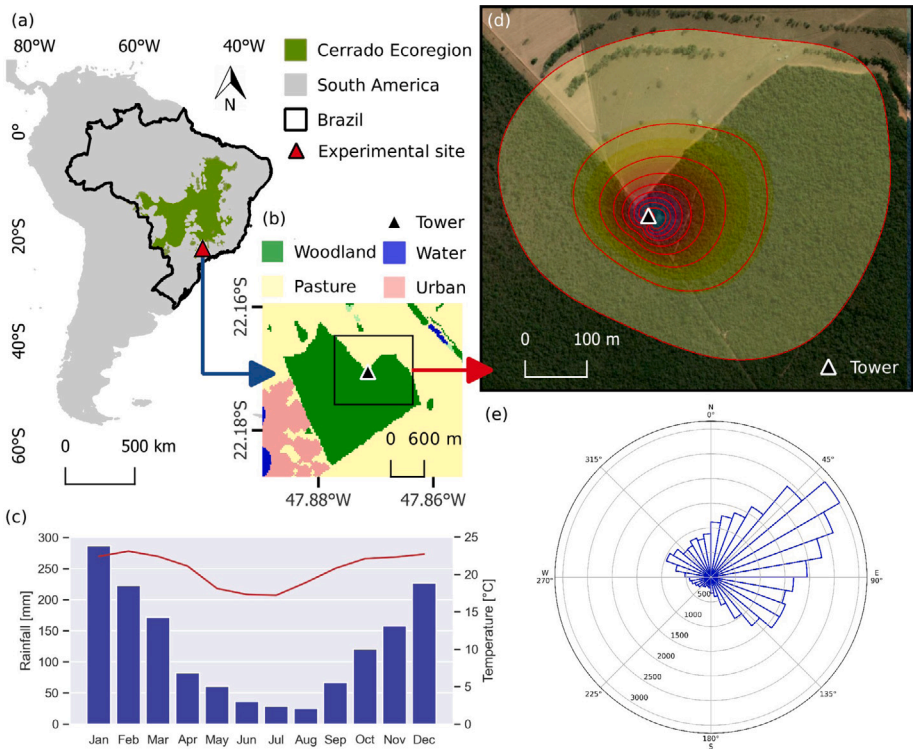

Fig. 2. (a) Experimental site's regional context; (b) Land cover in the flux tower surroundings; (c) Long-term average monthly rainfall and temperature in the study site; (d) Flux footprint along the monitoring period (10/2018-08/2021) calculated using two-dimensional method (Kljun et al., 2015); (e) Polar plot showing the wind direction histogram of the flux tower.

represent plant phenology). Additionally, selecting the optimal method (footprint-based or wind direction-based) to include source area information in the model is essential. For example, Holl et al. (2020) or Rößger et al. (2019) showed that partitioning EC data recorded over heterogeneous terrain is possible when flux contrasts are pronounced enough. Furthermore, we aim to contribute to the understanding of these systems' likely responses to projected future climatic change by leveraging the observed variability in environmental drivers, which were recorded in conjunction with our CO_2 flux observations over several years.

2. Methods

2.1. Site description

The experiment site is located in the city of Itirapina, within the state of São Paulo (22° 10.2517' S, 47° 52.2567' W) (Fig. 2a). The site's climate is classified as a humid subtropical climate, which has a warm and wet season from October to March and a cool and dry season from April to September (Alberton et al., 2014) (Fig. 2b). It has a mean annual precipitation of 1486 mm yr^{-1} and a mean annual temperature of 21.5 °C (Anache et al., 2019) (Fig. 2c). Predominantly, winds at the site came from east-northeastern directions (Fig. 2e).

The center of the study site is marked by a 24-meter-high flux tower, located within a natural wooded Cerrado (Alberton et al., 2014). The tower is adjacent to the boundary between a wooded Cerrado and a pasture (Fig. 2d). The wooded Cerrado has a six to seven meters tall woody component, with tree species including *Aspidosperma*, *Pouteria torta*, and *Caryocar* (Alberton et al., 2014; Felfili and da Silva, 1993). It does not have a continuous canopy, with tree cover ranging from 10 to 60 % (Alberton et al., 2014; Felfili and da Silva, 1993). Below the canopy, there is a continuous herbaceous layer (Alberton et al., 2014).

On the other hand, the pasture located north of the flux tower is mostly covered by 5 to 30 cm high signal grass (*Brachiaria decumbens*), with a small segment of sugarcane field to the northwest of the tower. The pasture part has been used for grazing since the 2000s (Anache et al., 2019). *Brachiaria decumbens*, originating from East Africa, is suitable for cattle grazing (Gorgone Barbosa et al., 2008). This perennial grass has a dense root system and a lifespan of approximately five years (Heuzé et al., 2021). It is also considered as an invasive species that inhibits the germination of other plants with its competitive advantages (Gorgone Barbosa et al., 2008).

2.2. Instrumentation

The micrometeorological variables were measured using slow (rainfall, temperature, relative humidity, net radiation, soil heat flux, and soil moisture at 1 Hz) and fast (wind speed and direction, H_2O and CO_2 molar fractions at 20 Hz) instrumentation (Table 1). The instruments were fixed on a 24-meter-high metal tower, which was equipped with a data acquisition and storage system. Despite the tower height, the main pieces of equipment were positioned below the maximum tower height due to footprint restrictions and lightning protection. The flux tower was operated between 2018 and 2021. The tower is listed with the site ID BR-IAB on the Ameriflux platform (https://ameriflux.lbl.gov/sites/siteinfo/BR-IAB) (AmeriFlux, 2024).

The EC system employed in this study underwent factory calibration prior to its initial deployment in the field (Campbell Scientific Irgason gas analyzer, see Table 1). To verify the accuracy of the gas analyzer, we conducted zero and span calibration procedures both before and after the monitoring period. These checks confirmed that no detectable drift occurred, ensuring the reliability of the measured values throughout the study. Additionally, the sensor lenses were cleaned every 21 days, coinciding with the scheduled data collection, to maintain optimal performance and ensure data quality.

Table 1
EC monitoring site instrumentation features.

Variable	Sensor	Height or depth* (m)	Measurement range	Accuracy
Temperature (°C)	HMP155A	16	−80 to +60 °C	±0.45 °C
Relative humidity (%)	HMP155A	16	0 to 100%	±1.7%
Rainfall (mm)	Hydrological Services TB4	16	0 to 700 mm h^{-1}	±3%
Atmospheric pressure (mbar)	Vaisala CS106	16	500 to 1100 mbar	±1.5 mbar
Wind speed (m s^{-1}) and direction (°)	Campbell Scientific Irgason sonic anemometer	16	0 to 30 m s^{-1}	±1.8 m s^{-1}
			0 to 360°	±0.7°
H_2O molar fraction	Campbell Scientific Irgason gas analyzer	16	0 to 72 mmol mol^{-1}	±2%
CO_2 molar fraction	Campbell Scientific Irgason gas analyzer	16	0 to 1000 μmol mol^{-1}	±1%
Soil moisture (%)	FDR EnviroSCAN Sentek	−0.3*	0 to ~65%	±3%
Net solar radiation (W m^{-2})	Kipp & Zonen CNR4	10	±2000 W m^{-2}	±20 W m^{-2}
Soil heat flux (W m^{-2})	Hukseflux HFP01	−0.1*	±2000 W m^{-2}	−15% to +5%

2.3. Eddy covariance data processing

Raw data processing and calculation of turbulent fluxes (latent heat flux, sensible heat flux, and CO_2 flux was performed using EddyPro version 7 (LI-COR Biosciences, 2021). Before flux processing, a dynamic metadata file was built, containing both time series of canopy height and displacement height, which were estimated using measured friction velocity (Pennypacker and Baldocchi, 2016) for each 30-min time interval. As an additional dynamic metadata time series, we prepared a dataset of wind sector-wise (2-degree sectors) binned and averaged roughness length estimates, calculated after (Kormann and Meixner, 2001), to reduce disturbances (noise, outliers) to the footprint model which could have been introduced by using instantaneous, half-hourly roughness length estimates per half-hourly footprint model run (same method has been applied by Holl et al. (2019b)). Thus, it was possible to account for land cover heterogeneity as well as dynamic vegetation development in the flux source area. The flux processing steps were: (i) raw data quality filtering (Vickers and Mahrt, 1997) including spike removal and filtering throughout the time series, considering signal strength and equipment detection limits; (ii) raw data processing including: double rotation method (Tanner and Thurteh, 1969); and time lag removal between concentration and wind measurements (Foken et al., 2012; Horst and Lenschow, 2009); (iii) raw flux calculation (iv) averaging and frequency corrections (Dijk, 2002; Foken et al., 2012; Horst and Lenschow, 2009; Kaimal et al., 1989; Moncrieff et al., 1997; Montgomery, 1947; Moore, 1986; Shapland et al., 2014); (v) conversion of the sonic sensible heat flux to sensible heat flux (Dijk, 2002; Schotanus et al., 1983); (vi) air density fluctuation correction (Webb et al., 1980); (vii) data quality control (Foken et al., 2012); (viii) spectral analysis and corrections (Mauder and Foken, 2004; Vickers and Mahrt, 1997; Moncrieff et al., 2005).

We then quality filtered the processed EC CO_2 flux data by omitting data points with quality class (QC) 1 and 2 (Mauder and Foken, 2004), those with an overall spectral correction factor (SCF) exceeding 1.1, and those with high CO_2 uptake value ($< -10\,\mu mol\,m^{-2}\,s^{-1}$) measured under low light conditions (photosynthetically active radiation (PAR) $< 10\ \mu mol\ m^{-2}\ s^{-1}$) (Runkle et al., 2013).

2.4. Eddy covariance footprint analysis

The half-hourly class contribution (CC) fraction of each investigated surface class to the EC flux was estimated by coupling the EC footprint model results with the land-use and land-cover product (LULC) (Souza et al., 2020). It was our initial purpose to use this information to enhance data quality by filtering out fluxes outside our initial area of interest (wooded Cerrado). We found that the CC time series could be utilized to characterize the contribution of each vegetation class, rather than discarding observations outside the primary area of interest. Initially, the footprint was computed utilizing a two-dimensional model (Kljun et al., 2015) at 30-min intervals, followed by normalization. Additionally, a pixel-specific threshold was established to confine the area subject to analysis. To prepare for the coupling between the flux footprint and LULC, we performed one hot encoding to generate binary matrices based on each vegetation class. In other words, each of the two analyzed classes received a numerical integer value, working as a masking layer to separate the footprint contribution of each class. Finally, a CC fraction was determined by integrating the footprint with the encoded LULC by summing up the half-hourly CC fractions of all pixels classified as belonging to one of the two investigated surface classes, respectively. This computation ensures that the observed data accumulates the combined contribution of the two compared classes within the footprint area: wooded Cerrado vegetation community and pasture (Fig. 2d).

2.5. Processing of meteorological data and auxiliary variables

First, we addressed gaps in the measured half-hourly air temperature (T_m, °C) records by filling them with debiased hourly ERA5-Land 2-meter air temperature (T_{era5}, °C) (Muñoz Sabater, 2019), following a simplified version of the gap-filling method employed by Lompar et al. (2019). Specifically, we first linearly interpolated the hourly T_{era5} data to half-hourly intervals. We then performed a linear regression analysis between the T_{era5} and the T_m, resulting in the relationship presented in Eq. (1). Afterward, we used the interpolated half-hourly T_{era5} data and Eq. (1) to estimate T_m and fill gaps in the measured half-hourly air temperature records.

$$T_m = 0.98 \times T_{era5} + 0.02374 \quad (1)$$

Following Holl et al. (2019a), we then calculated the monthly cumulative growing degree days (GDD) of the site with gap-filled air temperature data and a base temperature of 15 °C, which is a common choice when estimating the GDD of tropical and subtropical grasses, including *Brachiaria* (Andrade et al., 2016). GDD was defined as the sum of all positive differences between daily average temperatures and the base temperature.

Second, we calculated half-hourly PAR using measured shortwave irradiance, following Britton and Dodd (1976). We then filled the gaps in the calculated half-hourly PAR data (PAR_m) with debiased GeoNEX-based remote sensing PAR data (PAR_{GeoNEX}), derived from geostationary satellites and accessed via NASA's GeoNEX data portal (Li et al., 2023). Similar to the air temperature gap filling, we used linear regression to derive estimates for in situ measurements from the alternative data source, resulting in the relationship given in Eq. (2). The debiased PAR_{GeoNEX} data was then calculated to fill gaps in the PAR_m record.

$$PAR_m = 0.94 \times PAR_{GeoNEX} + 11.87 \quad (2)$$

Third, gaps in the measured half-hourly precipitation data were filled with 5-min precipitation data from a nearby site (22° 11.0847' S, 47° 51.1903' W), located 2.38 km southeast of the flux tower (Anache et al., 2024b). We summed 5-min measurements to obtain half-hourly totals. Subsequently, we adjusted the timestamps by adding 30 min to synchronize the gap-filling data with the measured data. We performed linear regression analysis and double mass analysis (Burton, 1985) to

evaluate the consistency between the gap-filling data and measured data (see Fig. D.16).

Additionally, we used Moderate Resolution Imaging Spectroradiometer (MODIS) Normalized Difference Vegetation Index (NDVI) estimates with a 16-day temporal resolution and a 250 m spatial resolution (Didan, 2021) to calculate the monthly NDVI for both ecosystems. We selected the center location of a wooded Cerrado (22° 10.6292' S, 47° 52.4907' W) and a pasture (22° 9.7692' S, 47° 52.0637' W) as points of interest to represent the NDVI of respective ecosystems. The original 16-day NDVI data was converted to monthly NDVI data by averaging the NDVI values within each month. The NDVI values, originally ranging from −2000 to 10000 (Didan, 2021), were scaled by multiplying by 0.0001. Afterward, we compared the modeled GPP of both ecosystems with their respective NDVI to validate the seasonal variability of the modeled GPP. Since the NDVI quantifies the greenness of the vegetation (U.S. Geological Survey, 2023), we expect the modeled GPP to exhibit similar seasonal variability as the NDVI.

Lastly, to characterize the photosynthesis efficiency of our two subsites, we calculated the monthly average light use efficiency (LUE) for both ecosystems using half-hourly modeled GPP of CO_2 and gap-filled PAR, following the method outlined by Alves et al. (2021) and using Eq. (3). The half-hourly GPP and PAR in μmol m^{-2} s^{-1} resulted in a unitless LUE. Monthly average LUE values were obtained by taking the mean of half-hourly LUE for each month.

$$LUE = \frac{GPP}{PAR} \tag{3}$$

2.6. Flux modeling

2.6.1. NEE component partitioning model (CPM)

We partitioned the measured NEE of CO_2 into its components, GPP and TER, using a combined photosynthesis–respiration model. The NEE component partitioning model (CPM), proposed by Runkle et al. (2013), combines a Michaelis–Menten-type hyperbolic light saturation function (Michaelis and Menten, 1913) to model the light response of photosynthesis (Zheng et al., 2012) with an exponential temperature model to estimate ecosystem respiration (van 't Hoff, 1900). The CPM (Eq. (4)) includes four parameters, each representing an EFP: maximum photosynthetic rate (P_{max}, μmol m^{-2} s^{-1}), initial quantum yield (α, unitless), base respiration (R_{base}, μmol m^{-2} s^{-1}), and temperature sensitivity coefficient (Q_{10}, unitless) (Runkle et al., 2013; Holl et al., 2019a).

$$\begin{aligned} NEE(T, PAR) &= -\frac{P_{max} \times \alpha \times PAR}{P_{max} + \alpha \times PAR} + R_{base} \times Q_{10}^{\frac{T-T_{ref}}{\gamma}} \\ &= -GPP(PAR) + TER(T) \end{aligned} \tag{4}$$

Following Holl et al. (2019a), we first divided the time series of measured NEE, air temperature, and PAR data into 36-day intervals (time windows) and optimized the CPM parameters for these intervals by minimizing squared model residuals using the SciPy Python module (Virtanen et al., 2020), particularly the function `curve_fit`. We set the reference temperature (T_{ref}) to 15 °C and γ to 10 °C, following Runkle et al. (2013) and Holl et al. (2019a). The boundaries for P_{max}, α, R_{base}, and Q_{10} were set as [0, 50], [0, 0.1], [0, 10], and [0, 5], respectively. The initial guess (p0) was set as follows: P_{max} at 30, α at 0.04, R_{base} at 4, and Q_{10} at 1.4. Following the curve fitting process, the 68% confidence interval (CI) for each EFP estimate was calculated from the covariance matrix (pcov) and used as an uncertainty estimate. EFP estimates with an uncertainty that exceeded half of their respective values were excluded. To fill the gaps in the estimated EFP time series resulting from quality filtering and missing NEE data, we used the mean of the corresponding estimated EFPs from the same month in other years. In cases where no value exists for the same month within the entire time series, we filled missing values with the mean of the EFPs from adjacent months. In the next step, we applied the Locally Weighted Scatterplot Smoothing (LOWESS) (Cleveland and Devlin, 1988) method to smooth the gap-filled EFP time series. This was achieved using the `lowess` function from the Python statsmodels library (Seabold and Perktold, 2010). We configured the `frac` parameter of the `lowess` function to 0.25. These smoothed EFP estimates were then interpolated to daily intervals using a second-order polynomial fit. Afterward, we calculated the root mean square error (RMSE) between the original EFP estimates and the smoothed EFP estimates. This RMSE value was used as an uncertainty estimate (95% CI) for the smoothed EFP estimates, which were propagated through the model equation to estimate uncertainties for modeled NEE, GPP, and TER, following Holl et al. (2019a). At last, we used these daily smoothed EFP estimates, along with gap-filled air temperature and PAR data, to drive the CPM model and partition NEE into GPP and TER.

2.6.2. Combined NEE component and source partitioning models

Since the EC flux tower was set up on the border between two contrasting ecosystems, the CO_2 fluxes measured by the EC sensors comprise signals originating from both the wooded Cerrado and the pasture. To separate these fluxes, we employed two strategies, namely an EC footprint analysis-based division (e.g. Holl et al. (2020); Rößger et al. (2019); Forbrich et al. (2011)), in which the relative contributions of both ecosystem types were included in the NEE component model as independent variables, as well as a simple wind direction-based division (e.g. Jammet et al. (2015)) of the dataset prior to NEE component modeling.

First, the EC footprint analysis-based division integrates the CPM with the CC, which is obtained through the footprint modeling, to model the NEE, GPP, and TER for both ecosystems. We named this approach CPM-F. Following the approach of Rößger et al. (2019), we fitted the measured NEE and modeled CCs, along with the measured meteorological data to Eq. (5) to estimate the EFPs for both ecosystems.

$$\begin{aligned} &NEE(T, PAR) = \\ &CC_{wood} \times \left(-\frac{P_{max,wood} \times \alpha_{wood} \times PAR}{P_{max,wood} + \alpha_{wood} \times PAR} + R_{base,wood} \times Q_{10,wood}^{\frac{T-T_{ref}}{\gamma}} \right) + \\ &CC_{pas} \times \left(-\frac{P_{max,pas} \times \alpha_{pas} \times PAR}{P_{max,pas} + \alpha_{pas} \times PAR} + R_{base,pas} \times Q_{10,pas}^{\frac{T-T_{ref}}{\gamma}} \right) \end{aligned} \tag{5}$$

Eq. (5) contains eight EFPs: a set of four for the wooded Cerrado, which includes $P_{max,wood}$, α_{wood}, $R_{base,wood}$, and $Q_{10,wood}$. There is another set of four for the pasture, comprising $P_{max,pas}$, α_{pas}, $R_{base,pas}$, and $Q_{10,pas}$. CC_{wood} and CC_{pas} denote the CC of wooded Cerrado and pasture, respectively. We applied fitting procedures similar to those used in CPM but with minor tweaks. Specifically, Q_{10} for both ecosystems were held constant at 1.4 to reduce model complexity and to avoid overfitting, following Mahecha et al. (2010) and Rößger et al. (2019). In addition, we used a 29-day time window and set the p0 for pasture's R_{base} to 3. With EFP estimates for both ecosystems, we proceeded to use gap-filled meteorological data to individually model the NEE, GPP, and TER for each ecosystem using CPM's model function (Eq. (4)). We also modeled the NEE of the entire site with CCs using Eq. (5).

Additionally, we combined the EC footprint analysis-based division approach with a stepwise component partitioning model (CPM-FS) proposed by Kutzbach et al. (2007) and Runkle et al. (2013) to model the NEE, GPP, and TER for both ecosystems. Specifically, we estimated EFPs in two steps by first estimating the R_{base} for both ecosystems by fitting the TER modeling function (Eq. (6)) to the NEE measured under low-light conditions (PAR < 20 µmol m^{-2} s^{-1}) (Runkle et al., 2013) with a 28-day time window. It assumes that the CO_2 fluxes measured under this condition are all ecosystem respiration (Runkle et al., 2013). We used the same curve fitting processes and settings as those used in CPM-F. With estimated R_{base} time series, we modeled TER of the entire site (TER_{all}) with gap-filled air temperature data and CCs using Eq. (6).

$$\begin{aligned} TER_{\text{all}}(T) &= CC_{\text{wood}} \times \left(R_{\text{base,wood}} \times Q_{10,\text{wood}}^{\frac{T-T_{\text{ref}}}{\gamma}} \right) \\ &+ CC_{\text{pas}} \times \left(R_{\text{base,pas}} \times Q_{10,\text{pas}}^{\frac{T-T_{\text{ref}}}{\gamma}} \right) \\ &= CC_{\text{wood}} \times TER_{\text{wood}} + CC_{\text{pas}} \times TER_{\text{pas}} \end{aligned} \quad (6)$$

In the second step, the GPP of the entire site (GPP_{all}) was calculated by subtracting the modeled TER_{all} from the measured NEE (Runkle et al., 2013). We then fitted calculated GPP, measured PAR and CCs to the GPP modeling function (Eq. (7)) based on the rectangular hyperbola function to obtain the estimated time series of P_{max} and α for both ecosystems using a 29-day time window. Combined with the estimated R_{base} obtained from the first step, we were able to model the NEE, GPP, and TER for both ecosystem types. Additionally, we summed modeled TER_{all} and GPP_{all} up to calculate the NEE of the entire site, which was compared with the measured NEE to evaluate the model performance.

$$\begin{aligned} GPP_{\text{all}}(PAR) &= CC_{\text{wood}} \times \left(-\frac{P_{\text{max,wood}} \times \alpha_{\text{wood}} \times PAR}{P_{\text{max,wood}} + \alpha_{\text{wood}} \times PAR} \right) \\ &+ CC_{\text{pas}} \times \left(-\frac{P_{\text{max,pas}} \times \alpha_{\text{pas}} \times PAR}{P_{\text{max,pas}} + \alpha_{\text{pas}} \times PAR} \right) \\ &= CC_{\text{wood}} \times GPP_{\text{wood}} + CC_{\text{pas}} \times GPP_{\text{pas}} \end{aligned} \quad (7)$$

For the second source partitioning strategy, we incorporated the wind direction-based division method with the CPM and named this approach CPM-WD. Specifically, we divided the measured NEE time series into two: wooded Cerrado's NEE and pasture's NEE, based on the wind direction measured by the tower at each half-hour timestep. Measured NEE with wind directions from 45° to 315° were categorized as wooded Cerrado's NEE, while those from 0° to 30° and 330° to 360° were classified as pasture's NEE (0° = 360° = North). In this way, measured NEE with wind directions from the boundary between the two ecosystems were excluded. With an NEE time series for each ecosystem type, we were able to estimate the EFPs for both by fitting the CPM's function with measured NEE and meteorological data. We used a 36-day time window and CPM-F's curve fitting settings for estimating EFPs, which then underwent the modeling procedures used in CPM and CPM-F to model the NEE, GPP, and TER for both ecosystems and the entire site.

2.7. Model performance evaluation and time window selection

We used the smoothing effectiveness metrics, including Akaike's information criterion (AIC), mean squared errors (MSE), bias error (BE), coefficient of determination (r^2), and RMSE, as a proxy for assessing model performance. The metrics' equations can be found on Appendix A. We expect the EFPs to exhibit a smooth pattern within natural systems. Therefore, a model with the most favorable smoothing effectiveness metrics is an indication of its capacity to effectively capture the expected smooth patterns beforehand, suggesting the model's better ability to model the fluxes.

To select an appropriate time window size for each NEE partitioning model, we tested a range of window sizes, varying from 1 to 60 days, while keeping other curve fitting settings constant across all four models, including CPM, CPM-F, CPM-FS, and CPM-WD. For each time window size tested, we conducted a comparison between the modeled NEE, which was obtained using that specific time window size, and the measured NEE by calculating the AIC, BE, r^2, and RMSE. The results of these comparisons can be found on Appendix E. Using these statistics, we studied how the time window sizes affect model performance and determined the optimal time window size. In addition to the performance metrics, we also took into account the smoothness of the estimated EFP time series to see if they represent natural plant development across different seasons. Estimated EFP time series obtained using the optimal time window for the four models are presented in Appendix F.

3. Results

3.1. Effects of data processing on temporal and spatial data coverage

Before quality filtering, 30707 processed EC CO_2 fluxes were available for a total of 50928 half hours during the observation period, hence 40% (n = 20221) half-hourly fluxes were missing. As shown in Fig. 3, most of these missing values resulted from two power outages: the first from 3 July 2019 to 5 December 2019 (accounting for 37% of missing values), and the second from 14 May 2021 to 30 July 2021 (accounting for 19% of missing values). After quality filtering, 24.14% (n = 7412) of the available data points (n = 30707) were omitted. This filtering process first excluded 23.88% (n = 7332) of the available data with a QC flag of 1 or 2. Additional filtering removed 0.24% (n = 74) of the points with a SCF greater than 1.1, and 0.02% (n = 6) of points measured under low light conditions with simultaneously large and thereby unrealistic CO_2 uptake.

After the quality filtering process, 23295 half-hourly CO_2 fluxes were available with non-zero contributions to the EC footprint from the wooded Cerrado as well as 20998 data points with non-zero contributions to the EC footprint from the pasture, respectively. The footprint-based component partitioning models we applied could leverage this comparatively large amount of data, although it contained mixed flux information. In comparison, with the wind direction sector-based data division, only half-hourly fluxes primarily related to one of the two ecosystems were used to deduct ecosystem-specific characterizations of the respective CO_2 flux dynamics. Therefore, only a limited subset of the measured fluxes could be leveraged to gain insight into ecosystem properties. In particular, based on the wind direction division, 15796 half-hourly fluxes were mainly associated with the wooded Cerrado, whereas only 5362 data points were mostly related to the pasture.

With footprint-based source partitioning, for both ecosystems a fairly evenly distributed amount of data points across the hours of the day is available. As shown in Fig. C.14, panel (a), both ecosystems exhibited a similar trend in hourly data distribution. Between 600 and 800 nighttime (17:00 to 08:00) data points were available for the wooded Cerrado, while the pasture followed a slightly lower but comparable pattern. During the daytime (09:00 to 16:00), a larger amount of data, ranging from 1000 to 1200, was available from both ecosystems. This increase in data points is the result of quality filtering, with a larger amount of data not fulfilling quality criteria, in particular tests for well-developed turbulence, during nighttime when turbulence creation is generally suppressed (see Fig. B.13) due to missing radiation input (e.g. Platter et al. (2024)). In contrast, with the wind direction-sector-based data division, differences in the hourly data coverage between the two sites are more pronounced (see Fig. C.15), with the pasture observations being slightly biased towards more nighttime measurements.

When examining the monthly distribution resulting from footprint-based data division, the number of data points for both ecosystems was similar, although slightly fewer data points were available for the pasture in all months. In general, fewer data points were available during the dry season months (July to September), as shown in Fig. C.14, panel (b). This reduction in data is primarily related to the measurement period, which runs from October 2018 to August 2021, resulting in less data for September compared to other months. Additionally, two power outage-related gaps in data collection further reduced the number of data points in the affected months, particularly in July.

Although the amounts of available flux observations are unevenly distributed on various time scales (see Figs. C.14 and C.15), we are confident that our dataset contained enough information on both ecosystems to characterize them accurately and fill observational gaps with models for the purpose of budget estimations. Our strategy of simultaneously modeling flux components from two ecosystems by utilizing EC footprint information removed biases in temporal data coverage (Fig. C.14 vs. Fig. C.15), that would otherwise have resulted from data

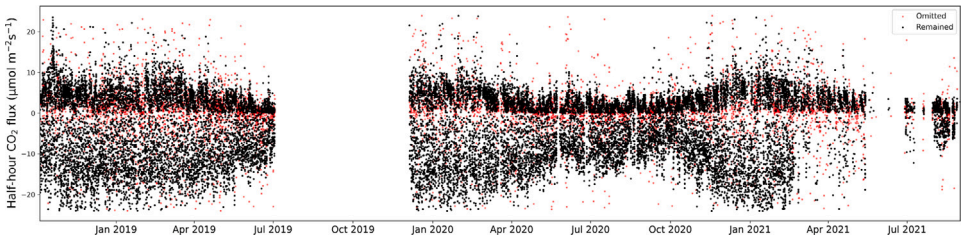

Fig. 3. Half hourly CO_2 fluxes measured at the study site from 5 October 2018 to 31 August 2021. Red dots mark the 7412 data points removed by the quality filtering. Black dots mark the remaining available data points.

division in wind sector-related fluxes. Given the higher availability of data related to the wooded Cerrado and due to the mixed nature of the management practices employed on the mixed agricultural site primarily used as a pasture, we are more confident in the robustness of the CO_2 flux estimates for the wooded Cerrado ecosystem type.

3.2. Analysis of meteorological data

The half-hourly air temperature data measured by the flux tower contains 29.20% (n = 14869) missing points. These gaps were entirely filled by the gap-filling process. To assess the fitness of the gap-filling data and the effectiveness of the debiasing process, we calculated the r^2 and RMSE for both raw T_{era5} data and debiased T_{era5} data. Both data achieved the same r^2 of 0.897. As for the RMSE, the debiased T_{era5} data had a value of 1.552 °C, which was lower than the raw T_{era5}'s 1.602 °C, indicating a closer alignment with the measured data. Overall, the debiased T_{era5} data demonstrated good agreement with the measured air temperature.

The half-hourly PAR_m data contains 18.73% (n = 9537) missing values. The gap-filling process filled these gaps entirely with debiased PAR_{GeoNEX} data, which showed good agreement with PAR_m. The linear regression analysis shows that the debiased PAR_{GeoNEX} data had a high r^2 value of 0.915 and an RMSE of 179 μmol m^{-2} s^{-1}. Compared to the raw PAR_{GeoNEX} data, the debiasing process decreased RMSE by 2.19% while maintaining the same r^2 value.

The half-hourly measured precipitation data at the site contained 18.73% (n = 9537) gaps and was filled entirely by the gap-filling process (Fig. B.12(a)). The gap-filling precipitation data was summed into monthly totals and compared with the measured monthly cumulative precipitation data. It displayed adequate agreement with a r^2 of 0.63 and an RMSE of 77 mm. A further double mass analysis also demonstrated adequate agreement between the two as the slope of the double mass curve is close to the identity line (See Appendix D).

The half-hourly evapotranspiration (ET) data at the site contained 30.39% (n = 15478) gaps. We first omitted those data with a QC 1 or 2 (Mauder and Foken, 2004), which removed 11806 data points. Additional filtering excluded values below 0 mm/hr and above 1 mm/hr, removing a further 1990 data points. After filtering, 21654 data points remained, representing 42.52% of the total 50928 data points expected for the entire study period (Fig. B.12(b)). Additionally, we calculated the ratio of monthly cumulative ET to precipitation (ET/P) using filtered half-hourly ET and gap-filled precipitation (Fig. B.12(c)). Monthly ET/P values were included only when at least 7 days of half-hourly ET data were available within the month.

In the comparison of the NDVI for the wooded Cerrado and pasture, the wooded Cerrado consistently showed a higher NDVI. Specifically, the mean NDVI for wooded Cerrado was 0.8, which was 35% higher than the mean for the pasture. Throughout the study period, and thereby throughout several vegetation periods, the NDVI for the wooded Cerrado remained relatively stable at around 0.8, with minor reductions during the dry months of July and August (Fig. 5a). In contrast, the NDVI for the pasture exhibited higher seasonal variability, with values reaching around 0.7 during the wet seasons and declining to around 0.4 in dry seasons (Fig. 5b). Furthermore, the SD of NDVI for the pasture was 129% higher than that of the wooded Cerrado, indicating a greater degree of seasonal variability.

To better characterize the inter-annual variability of environmental conditions at our site, we divided the gap-filled meteorological data described above, including air temperature, GDD, PAR, precipitation, ET, ET/P, and NDVI, into three 10-month periods (Table 2). Each period spanned from November 1st to August 31st of the following year. Due to the absence of in situ data for September and October 2021, we excluded all data from these months in all other years to ensure uniformity in the length of three periods for comparative analysis. Regarding ET, due to the extent of gaps and the lack of a gap-filling process (which would require significant additional analysis beyond the scope of this study), we summed filtered ET data to daily totals and calculated mean, median, and SD of daily total ET for each period to provide a general view (Table 2). Additionally, we estimated cumulative ET separately for both the wet and dry seasons in each period by multiplying the mean daily total ET of the corresponding season by the number of days in each season (Table 2). Using these values, we then calculated cumulative ET/P ratios for each period, as well as for the wet and dry seasons individually (Table 2). It is important to state that the ET reported here represents the land cover of the entire flux footprint, mixing wooded Cerrado and pasture at the same values.

3.3. Carbon dioxide flux modeling results

3.3.1. Model performance evaluation and selection

We selected the results of CPM-F for our analysis after evaluating the model performance metrics of three NEE component partitioning models with source partitioning capability. Although all three models demonstrated similar performance levels, CPM-F edged out the other two by exhibiting the most favorable AIC, MSE, RMSE, and BE values (Table 3). Compared to CPM-F, the CPM-FS allocated all flux under low light conditions to TER, which could potentially skew the estimation of EFPs and lead to inferior performance. On the other hand, the CPM-WD model was constrained by the wind direction source partitioning method, resulting in poorer performance. It was unable to exclude all the fluxes from the wooded area based on wind direction alone. Specifically, the wind direction range used to exclude the fluxes from the wooded area for estimating the EFPs of the pasture still includes some wooded areas on the eastern and northern sides, potentially skewing the results. Regardless of how the range is set, it cannot completely exclude all fluxes from wooded areas, and a strict narrow range would result in insufficient data points to estimate EFPs for the pasture.

3.3.2. Overview of carbon flux and seasonal dynamics from model results

We examined the modeled GPP-C (gross carbon uptake via GPP, g m^{-2}), TER-C (gross carbon release via TER, g m^{-2}), and NEE-C for both ecosystems using CPM-F. Initially, we found that the GPP-C and TER-C of both ecosystems shared a similar seasonality, peaking in the wet season around January and reaching minimum values during the dry season in July. Over the entire study period, the wooded Cerrado's

Table 2
Summary of processed meteorological data. The table shows key meteorological variables and indices organized into three 10-month periods (November 1st to August 31st of the subsequent year), denoted as Period 1 (P1), Period 2 (P2), and Period 3 (P3). Each period is further divided into a wet season from November to March and a dry season from April to August. Statistics include total, mean, median, and SD values for each period and season.

		Period 1 (P1) (2018-11-01 to 2019-08-31)	Period 2 (P2) (2019-11-01 to 2020-08-31)	Period 3 (P3) (2020-11-01 to 2021-08-31)
Air temperature (°C)	Mean	21.41	20.95	20.78
	Median	21.86	21.19	21.30
	SD	3.16	2.75	3.24
	Wet season mean (November to March)	23.30	22.72	23.00
	Dry season mean (April to August)	19.55	19.19	18.61
GDD (°C)	Total	1973	1828	1792
	Mean monthly sum	197	183	179
	Wet season total (November to March)	1253	1174	1208
	Dry season total (April to August)	721	655	584
PAR (mol m^{-2})	Total	11 183	11 202	11 393
	Wet season total (November to March)	6174	6000	6395
	Dry season total (April to August)	5009	5202	4998
Precipitation (mm)	Total	1016	1519	648
	Wet season total (November to March)	807	1366	592
	Dry season total (April to August)	209	153	56
ET (mm day^{-1})	Mean	2.817	2.441	1.783
	Median	2.840	2.263	0.992
	SD	0.957	1.076	1.622
ET (mm)	Total	814	766	442
	Wet season total (November to March)	492	473	385
	Dry season total (April to August)	322	293	57
ET/P	Total ratio	0.80	0.50	0.68
	Wet season ratio (November to March)	0.61	0.35	0.65
	Dry season ratio (April to August)	1.54	1.92	1.02
NDVI Wooded Cerrado	Mean	0.8050	0.8027	0.7804
	SD	0.0413	0.0253	0.0874
NDVI Pasture	Mean	0.5958	0.5693	0.5441
	SD	0.1145	0.0902	0.1692

Table 3
Comparison of model performance metrics for three NEE component partitioning models with source partitioning capability and the CPM without source partitioning.

	CPM-F	CPM-FS	CPM-WD	CPM
AIC	55 783	55 913	55 909	55 015
MSE	10.96	11.02	11.02	10.60
r^2	0.84	0.84	0.84	0.85
RMSE	3.31	3.32	3.32	3.26
BE	0.0105	0.0128	−0.2874	−0.1247

Table 4
Mean and SD of daily GPP-C, TER-C, and NEE-C in for both ecosystems (g m^{-2} d^{-1}).

		Wooded Cerrado	Pasture
Mean	GPP-C	6.23	5.11
	TER-C	4.48	4.38
	NEE-C	−1.75	−0.73
SD	GPP-C	2.04	2.27
	TER-C	1.53	1.52
	NEE-C	1.06	1.38

mean daily GPP-C and TER-C were 6.23 g m^{-2} d^{-1} and 4.48 g m^{-2} d^{-1}, which was 22% and 2% higher than those for the pasture (Table 4).

Both ecosystems could reach similar peak GPP-C values around 10 g m^{-2} d^{-1} during the wet seasons (Fig. 4). However, during each dry season within the study period, the pasture consistently displayed lower minimum GPP-C values compared to the wooded Cerrado. As depicted in Fig. 4, during the dry seasons, the wooded Cerrado's GPP-C mostly hovered around 4 g m^{-2} d^{-1} to 5 g m^{-2} d^{-1}. In contrast, the GPP-C of the pasture was generally around or below 3 g m^{-2} d^{-1}. In terms of NEE-C, both ecosystem types acted as carbon sinks for the majority of the study period. Specifically, out of 1061 days of data, the wooded Cerrado acted as a sink for approximately 94% (996 days) of the time, while the pasture acted as a sink for around 73% (770 days) of the time.

3.3.3. Model result validation

To assess the plausibility of our results, we compared the modeled GPP-C time series of both ecosystems with their respective NDVI values. In theory, the modeled GPP-C should have a similar seasonal course as the NDVI. We found that the GPP-C for the pasture showed good agreement with its NDVI in terms of seasonality (Fig. 5). Both had a high seasonal variability and similar timing of peaks and minima most of the time. However, the modeled GPP-C for the wooded Cerrado exhibited a discrepancy with its NDVI in terms of seasonality. While the seasonality of the wooded Cerrado's GPP-C was pronounced, its NDVI showed less variation. This discrepancy may arise from the dominance of evergreen tree species in the wooded Cerrado, whose NDVI remains relatively constant throughout the year (Table 2). In contrast, the GPP-C of the wooded Cerrado fluctuated strongly due to variations in meteorological conditions across different seasons, which caused the discrepancy. Alternatively, there is a possibility that our model overestimated the seasonality. To exclude this possibility, we used a

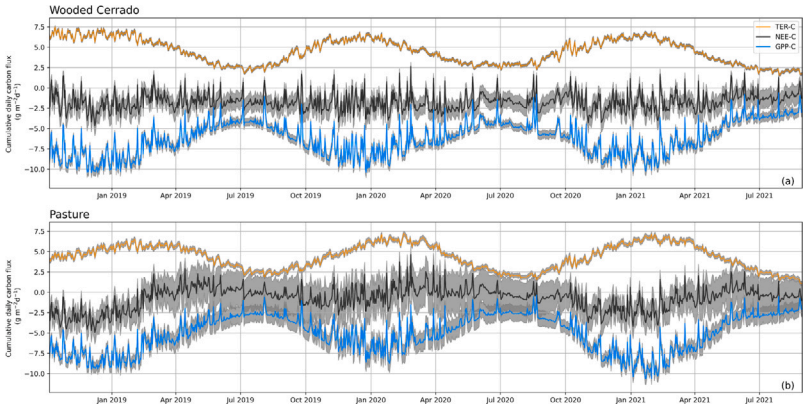

Fig. 4. Time series of daily summed TER-C, NEE-C, GPP-C, and their associated uncertainties (95% CI) for both wooded Cerrado (a) and pasture (b) in grams of carbon per square meter per day (g m^{-2} d^{-1}) modeled using CPM-F. Values with a negative sign indicate carbon uptake.

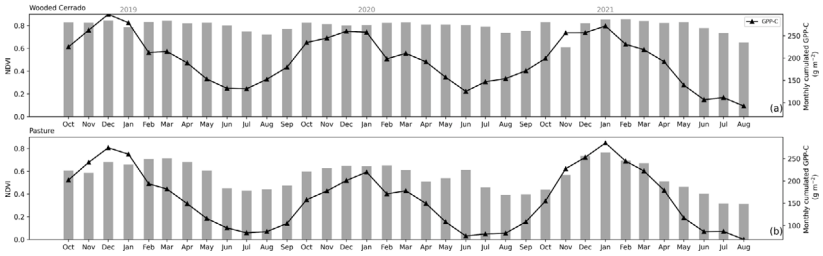

Fig. 5. Time series of monthly NDVI and monthly cumulated GPP-C for wooded Cerrado (a) and pasture (b).

larger 180-day time window to estimate the EFPs and modeled GPP-C for the wooded Cerrado. By methodologically reducing the temporal variability of EFPs in this way, we aimed to artificially yield a flatter course of the GPP-C time series, resembling the NDVI time series more closely. However, this approach led to a high AIC and lower r^2 values, indicating worse model performance. Hence, it is unlikely that the overestimation of seasonality was the case.

Furthermore, to test the impact of model complexity on the modeled component flux time series, we compared the results from our CPM-F approach for the wooded Cerrado with the results from our CPM model, which estimates GPP-C, TER-C, and NEE-C for the entire site without source partitioning and differentiating between areas under different management. Since signals from the wooded Cerrado dominate the EC footprint most of the time, we expect the results from the simpler CPM model to be of comparable magnitude and show similar dynamics to the CPM-F results relating to the wooded Cerrado only. We found that the CPM-F results for the wooded Cerrado showed good agreement with CPM results in terms of both seasonality and magnitude (Fig. 6). CPM-F's estimates for wooded Cerrado's TER-C and GPP-C were slightly higher than the respective estimates from the CPM approach. We found this difference to be reasonable, given that CPM models the whole site, comprising a mixture of wooded Cerrado and pasture. The lower mean daily GPP-C and TER-C of the pasture compared to the wooded Cerrado (Table 4) contributed to the modeled GPP-C and TER-C using CPM being lower than those purely representing the wooded Cerrado as obtained by CPM-F.

3.4. Annual fluxes and inter-annual variability

Our results show that while both sites functioned as annual carbon sinks, the wooded Cerrado showed greater carbon sequestration capability than the pasture. Over the entire 35-month study period, the wooded Cerrado sequestered approximately 1084 g m^{-2} (140%) more carbon than the pasture. Despite similar cumulative TER-C, the wooded Cerrado's cumulative GPP-C exceeded that of the pasture by 1189 g m^{-2} (22%), resulting in wooded Cerrado's higher carbon uptake during the entire study period. In addition, we used complete NEE-C data from 2019 and 2020 to calculate and compare two complete annual cumulative NEE-C values for both areas of interest. We again found that the wooded Cerrado was the stronger cumulative carbon sink of the two sites. The wooded Cerrado's annual NEE-C amounted to −639 ±20 g m^{-2} yr^{-1} and −673 ±19 g m^{-2} yr^{-1} for 2019 and 2020, respectively. They were 338% and 276% higher than the annual NEE-C balance from the pasture, which amounted to −146 ±39 g m^{-2} yr^{-1} and −179 ±38 g m^{-2} yr^{-1} (Table 5), respectively. The substantial difference in annual NEE-C is attributed to the wooded Cerrado's higher annual GPP-C compared to the pasture. Specifically, while annual TER-C remained similar between the two ecosystems for both years, wooded Cerrado's annual GPP-C was 32% and 28% higher than the pasture's in 2019 and 2020, respectively. Additionally, the higher precipitation observed in 2020 increased NEE-C uptake for both ecosystems (Table 5).

We divided the time series of GPP-C, TER-C, and NEE-C for both sites into three periods and separated them into dry and wet seasons to further analyze their inter-annual and seasonal variability (Table 6). We found that the wooded Cerrado's stronger annual carbon sink function can be traced back to its larger dry season net carbon uptake. Specifically, the wooded Cerrado's average dry season NEE-C was −244 g m^{-2}, substantially surpassing the pasture's −1.35 g m^{-2}. This difference arose due to wooded Cerrado's average dry season GPP-C being 195 g m^{-2} (39%) larger than the pasture's GPP-C, coupled with a slightly lower average dry season TER-C of 47 g m^{-2} (9%). This resulted in a net difference of 242.65 g m^{-2} in carbon uptake during the dry season between the two sites. This finding is consistent with Silva et al. (2006), who claim that native Cerrado vegetation can maintain higher GPP-C during the dry season due to their deeper roots, which allow them to utilize deeper soil water.

During the wet season, the pasture's NEE-C was more comparable to the wooded Cerrado's. However, the wooded Cerrado's average wet season NEE-C of −297 g m^{-2} was still 48.5% larger than the pasture's,

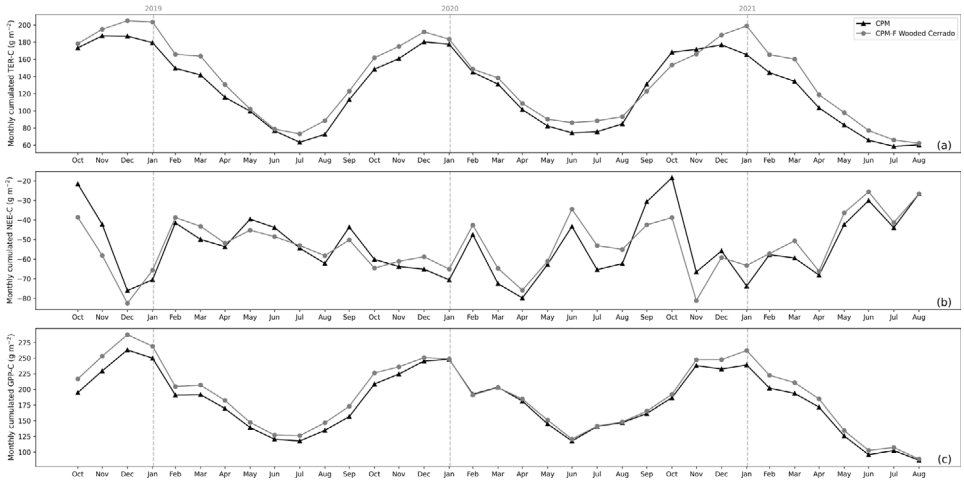

Fig. 6. Comparison of monthly cumulated TER-C (a), NEE-C (b), and GPP-C (c), between CPM and CPM-F's results for the wooded Cerrado.

Table 5
Cumulative CO_2 fluxes (NEE-C, GPP-C, TER-C) for the wooded Cerrado and pasture ecosystems in 2019, 2020, and over the entire 35-month study period, expressed in g m^{-2} yr^{-1} for annual values and in g m^{-2} for the entire period. Annual precipitation (mm) and ET (mm) are also included to provide additional context for the environmental conditions during the study period. The cumulative ET for 2019, 2020, and the entire study period are calculated using the average daily total ET for each year and for the entire period, multiplied by the number of days in each respective period.

		2019	2020	Entire
Wooded Cerrado	NEE-C	−639 ± 20	−673 ± 19	−1859 ± 34
	GPP-C	2297 ± 9	2241 ± 9	6610 ± 16
	TER-C	1658 ± 3	1568 ± 3	4750 ± 6
Pasture	NEE-C	−146 ± 39	−179 ± 38	−775 ± 63
	GPP-C	1741 ± 19	1745 ± 18	5421 ± 30
	TER-C	1594 ± 5	1566 ± 5	4646 ± 9
Entire study area	Precipitation	1238	1731	3451
	ET	574	836	2469

due to its higher average wet season GPP-C. In addition, the pasture showed greater inter-period variability in wet season NEE-C by having a SD of 124 g m^{-2} across the three periods, which was substantially larger than wooded Cerrado's 10 g m^{-2}. Overall, wooded Cerrado's stronger GPP-C in both seasons, coupled with a slightly lower average TER-C in the dry season and similar TER-C in the wet season, makes it the stronger carbon sink of the two ecosystems.

3.5. Diurnal cycles of net carbon dioxide fluxes

We calculated the average diurnal cycles for both areas of interest during the wet and dry seasons of 2019 and 2020, respectively. We found similar diurnal patterns, but different magnitudes of daytime NEE-CO_2 uptake (Fig. 7). Both ecosystems reached their peak NEE-CO_2 uptake around 11:30 am to 12:00 pm, after which it decreased, turning into a source of CO_2 around 5:30 pm. During the nighttime, both ecosystems showed similar NEE-CO_2 levels in both years. However, the wooded Cerrado exhibited substantially higher daytime uptake than the pasture in both seasons. Specifically, during the wet season, the wooded Cerrado's highest daytime NEE-CO_2 uptake could reach -14 μmol m^{-2} s^{-1} in both years, while the pasture could only reach -11 μmol m^{-2} s^{-1} for both years. During the dry season, the difference in maximum daytime NEE-CO_2 uptake between the two ecosystems became larger. For both years, while the wooded Cerrado could reach around -11 μmol m^{-2} s^{-1}, the pasture only hovered around -6 μmol m^{-2} s^{-1}.

In summary, similar to the pattern we found for the annual component fluxes, the pasture showed larger seasonal variability in CO_2 fluxes. We observed that the pasture displayed more seasonal variations and was more bound to seasonal changes in environmental variables. On the other hand, the wooded Cerrado was less susceptible to seasonal environmental variable changes and was able to maintain a higher NEE-CO_2 daytime uptake during the dry season.

3.6. Comparison of light use efficiency between sites

We found that the two ecosystems' LUE had similar seasonality but different magnitudes. First, in terms of seasonality, LUE decreased at both sites in the dry season and reached their lowest LUE of the year around July to August (Fig. 8). From there, both ecosystems' LUE started to increase and reached their wet season peak around January. Second, in terms of magnitude, the pasture's LUE was similar to the wooded Cerrado's LUE during the wet seasons, but much lower than the wooded Cerrado's LUE during the dry seasons. Specifically, in the wet season, the wooded Cerrado's mean wet season LUE was 0.022, which was about 16% higher than the pasture's 0.019. During the dry season, the difference between the two increased. The wooded Cerrado had a substantial 40% higher average dry season LUE than the pasture (Table 7). Moreover, the pasture's dry season lowest LUEs were below 0.01, which were substantially lower than the wooded Cerrado's dry season minima. The LUE time series of both ecosystems followed a similar pattern to the ET time series (Fig. B.12(b)), with higher LUE values occurring during the wet season when ET also peaked. In short, the wooded Cerrado was more efficient in using PAR than the pasture, especially in the dry seasons, allowing it to keep a higher GPP and NEE.

3.7. Flux-environmental variable relations

We additionally analyzed how the variability of environmental variables, as well as proxies for the latter, including precipitation, air temperature, GDD, and PAR, changed over the three investigation periods and how they could have affected the discussed carbon dynamics. This analysis showed the processes leading to CO_2 exchange fluxes were more susceptible to changes in environmental variables at the pasture than at the wooded Cerrado.

First, from P1 to P2, precipitation increased substantially while mean air temperature, GDD, and cumulative PAR decreased slightly. Specifically, the most substantial difference between the two periods in terms of environmental variables was the increase in total precipitation. P2 had 503 mm, which is 49% more total precipitation than P1. In particular, P2 had 69% (559 mm) more wet season precipitation than P1 due to the heavy rain in P2's February, which was the main cause of P2's high annual precipitation. The increase in wet season precipitation in P2 coincided with a decrease in wet season PAR, which was 3%

Table 6
Three periods' total GPP-C, TER-C, and NEE-C in grams per square meter (g m^{-2}) with their uncertainties for both ecosystems. Each period's total GPP-C, TER-C, and NEE-C were partitioned into its dry and wet season components. The mean and SD of three periods' total, dry, and wet season GPP-C, TER-C, and NEE-C were also listed.

			P1	P2	P3	Mean	SD
Wooded Cerrado	GPP-C	Wet season	1221 ± 6	1130 ± 6	1190 ± 6	−1180	38
		Dry season	730 ± 6	747 ± 6	618 ± 6	698	57
		Total	1951 ± 8	1876 ± 8	1809 ± 9	1879	58
	TER-C	Wet season	933 ± 2	837 ± 2	879 ± 2	883	39
		Dry season	473 ± 2	467 ± 2	422 ± 2	454	23
		Total	1406 ± 3	1304 ± 3	1301 ± 3	1337	49
	NEE-C	Wet season	−288 ± 13	−292 ± 13	−311 ± 13	−297	10
		Dry season	−257 ± 12	−280 ± 12	−196 ± 13	−244	35
		Total	−545 ± 18	−572 ± 17	−507 ± 19	−541	26
Pasture	GPP-C	Wet season	1110 ± 9	913 ± 13	1188 ± 9	1070	116
		Dry season	510 ± 13	480 ± 13	518 ± 12	503	16
		Total	1620 ± 15	1393 ± 18	1706 ± 15	1573	132
	TER-C	Wet season	819 ± 3	888 ± 3	903 ± 3	870	37
		Dry season	555 ± 3	463 ± 3	487 ± 3	501	39
		Total	1374 ± 5	1351 ± 5	1389 ± 5	1372	16
	NEE-C	Wet season	−291 ± 19	−24 ± 26	−285 ± 19	−200	124
		Dry season	45 ± 26	−17 ± 27	−32 ± 25	−1.35	33
		Total	−247 ± 32	−42 ± 38	−317 ± 31	−202	117

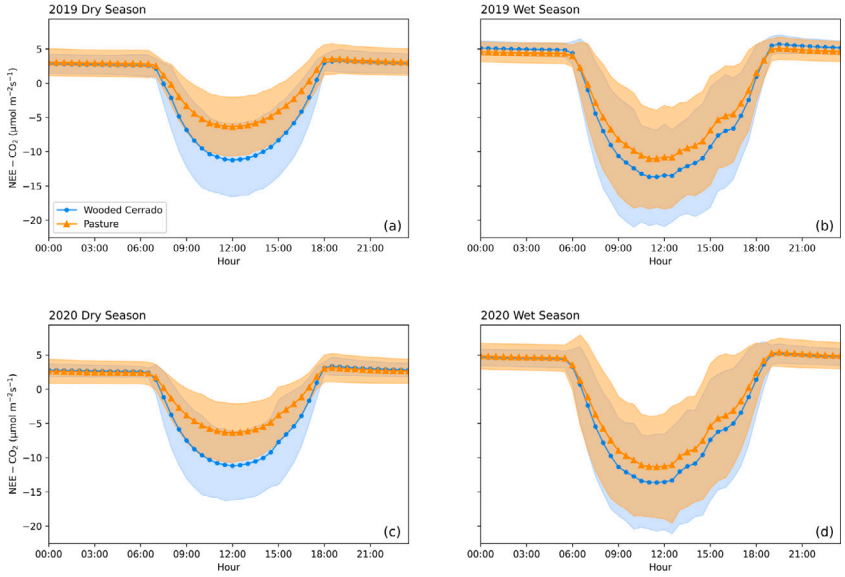

Fig. 7. Average diurnal cycles of NEE-CO_2 during the dry and wet seasons of 2019 and 2020 for wooded Cerrado and pasture. The shaded area represents the uncertainty estimates (95% CI), calculated as two times the SD of NEE-CO_2 groups aggregated by half-hour intervals for the entire year.

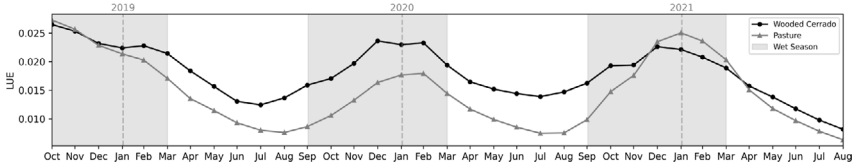

Fig. 8. Monthly average LUE for both ecosystems from October 2018 to August 2021. The wet seasons from October to March are denoted by the gray shade.

Table 7
Mean and SD of LUE for both ecosystems during both seasons.

	Wet season mean	Dry season mean	Total mean	SD
Wooded Cerrado	0.022	0.014	0.018	0.0046
Pasture	0.019	0.010	0.015	0.0062

lower than P1 (Table 2). Additionally, the ET/P ratio declined from 0.80 to 0.50, largely due to the higher precipitation in P2 (Table 2). However, P2's dry season PAR was 4% higher than P1, resulting in almost identical total cumulated PAR for both periods.

For the wooded Cerrado, under these changes in environment variables, its total NEE-C uptake increased by 5% in P2 (Table 6). While its P2 dry season GPP-C was similar to P1's, its P2 wet season GPP-C had a 7% decrease, resulting in a 4% lower total period GPP-C. We speculate that the wooded Cerrado's GPP-C was not limited by precipitation in the wet season. Instead, the additional wet season precipitation in P2 led to lower PAR in December, January, and February of P2, which eventually decreased its wet season GPP-C. On the other hand, its wet season total TER-C decreased by 10% from P1 to P2, which could be caused by the lower mean air temperature and wet season GDD in P2. The decrease in wet season TER-C compensated for the decrease in

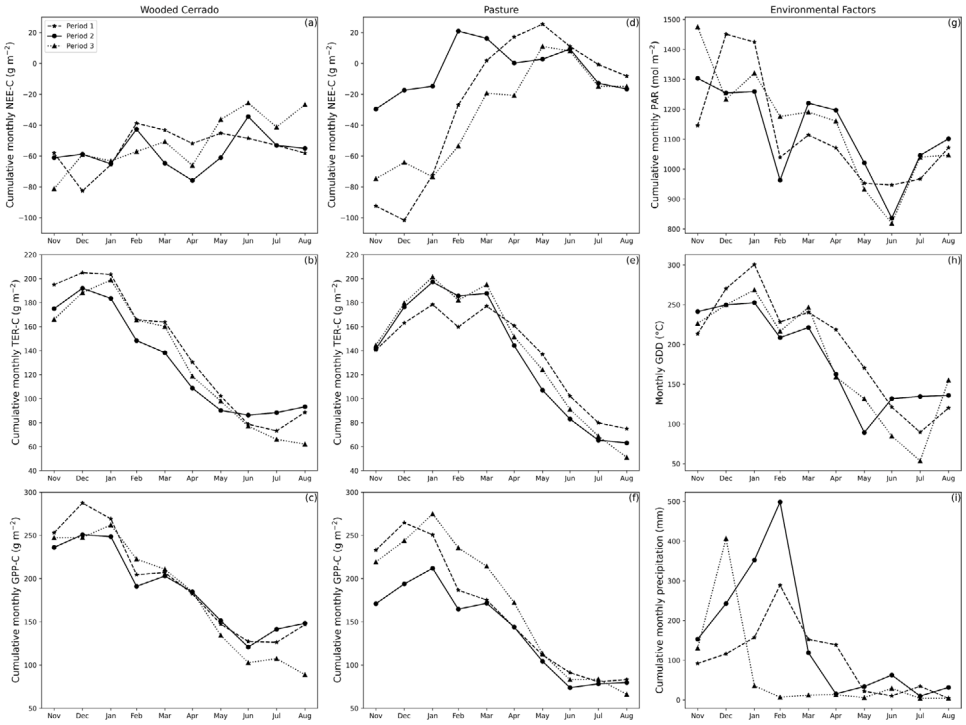

Fig. 9. Comparison of monthly cumulative carbon fluxes and environmental factors across three investigation periods (P1, P2, and P3) for both areas of interest. The first column, panels (a) to (c), shows the monthly cumulative NEE-C, TER-C, and GPP-C for wooded Cerrado. The second column, panels (d) to (f), shows the same flux variables for the pasture. The third column, panels (g) to (i), shows the monthly cumulative PAR, GDD, and precipitation across the investigation periods.

GPP-C and resulted in an overall increase in total NEE-C in P2 for the wooded Cerrado.

In contrast, the total NEE-C at the pasture saw a drastic decrease of 83% in P2, primarily due to a substantial reduction in the wet season GPP-C. Notably, unlike the trend observed at the wooded Cerrado, both the wet and dry season GPP-C at the pasture decreased by 18% and 6%, respectively. This suggests that the pasture was strongly affected by the increased precipitation and other environmental factor changes during P2. Meanwhile, its total TER-C exhibited only a slight decrease of 1.7% in P2, failing to compensate for the decrease in GPP-C and resulting in the decrease of NEE-C in P2 (see Fig. 9).

Upon examining the environmental factor changes from P2 to P3, we observed a substantial decrease in wet season precipitation, alongside minor changes in total GDD and PAR. Both the wet and dry seasons in P3 saw a substantial decrease in precipitation by 57% and 63%, respectively, which resulted in a total 871 mm (57%) decrease in precipitation for the period (Table 2). Additionally, the ET/P ratio increased from 0.50 to 0.68 (Table 2). Meanwhile, the cumulated PAR during the wet season rebounded in P3, showing a 7% increase (Table 2).

In response to these environmental factor changes, the total NEE-C uptake for the wooded Cerrado decreased by 11.36% in P3, moving from −572 ±17 g m^{-2} to −507 ±18 g m^{-2} (Table 6). While the total wet season NEE-C remained almost unchanged, the dry season NEE-C saw a 30% decrease, mainly due to a 17% reduction in its dry season GPP-C. Meanwhile, the wet season GPP-C of the wooded Cerrado was almost unaffected by the decrease in wet season precipitation. This observation, combined with our findings from P1 to P2, demonstrates that the wooded Cerrado is strongly resistant to changes in precipitation during the wet season. However, during the dry season, the reduced precipitation in P3 did lead to a decrease in its dry season GPP-C, thereby resulting in a lower NEE-C for the period.

In contrast, the pasture had a substantial 655% increase in total NEE-C in P3, moving from −42 ±38 g m^{-2} to −317 ±31 g m^{-2}. In P3, the pasture's total GPP-C increased by 313 g m^{-2} (22%), while its total TER-C only increased slightly by 38 g m^{-2}, leading to a substantial increase in its total NEE-C (Table 6). Interestingly, the pasture's total wet season GPP-C increased by 30% in P3, despite it being the period with the lowest wet season precipitation of the three investigation periods. On the other hand, its total dry season GPP-C in P3 remained close to P2's value, even though P3 had the lowest dry season precipitation of the three periods. These observations indicate that the vegetation at the pasture site is resilient to drought to some degree for both seasons, but is more vulnerable to excessive precipitation in the wet season.

4. Discussion

4.1. Comparison of the wooded Cerrado to other woodland ecosystems

Compared to previous EC studies on NEE in wooded Cerrado, including those by Miranda et al. (1996), Miranda et al. (1997), and da Rocha et al. (2002), our wooded Cerrado site exhibited a higher annual NEE-C uptake, primarily due to higher dry season NEE-C uptake. Specifically, during the dry season months of July and August, da Rocha et al. (2002) reported that wooded Cerrado turns into a carbon source, with an average daily NEE-C of 2.70 g m^{-2} d^{-1} and 1.95 g m^{-2} d^{-1}, respectively (Vourlitis and da Rocha, 2010). Meanwhile, Miranda et al. (1996) found that the NEE-C uptake of wooded Cerrado decreases during the dry season but remains a minor sink, with average daily NEE-C around −0.64 g m^{-2} d^{-1} and −0.13 g m^{-2} d^{-1} for July and August, respectively (Vourlitis and da Rocha, 2010). In contrast, our results indicate that the wooded Cerrado maintains its role as a strong carbon sink during the dry season, with daily average NEE-C uptake around −1.5 g m^{-2} d^{-1}. During the wet season months, such as November, December, and January, our modeled NEE-C is close to those of Miranda et al. (1997) and da Rocha et al. (2002), showing NEE-C uptake around −2 g m^{-2} d^{-1} (Fig. 10) (Vourlitis and da Rocha, 2010).

We also compared our results with the study by Vourlitis et al. (2001) regarding the NEE-C in a mature Amazonian transitional tropical forest known as cerradão, which is a variant of the Cerrado biome

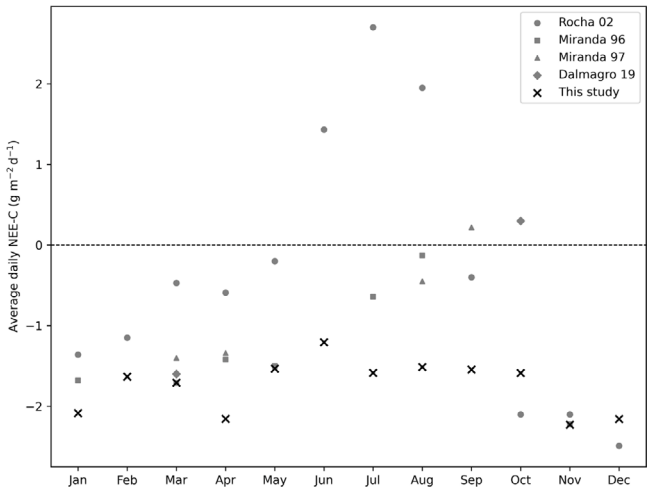

Fig. 10. Comparison of average daily NEE-C fluxes from this study with values from similar Cerrado ecosystems described in previous studies by da Rocha et al. (2002) (Rocha 02), Miranda et al. (1996) (Miranda 96), Miranda et al. (1997) (Miranda 97), and Dalmagro et al. (2019) (Dalmagro 19). The average daily NEE-C values for each month from this study were calculated by averaging over the entire study period. The average daily NEE-C values of Rocha 02, Miranda 96, and Miranda 97 were extracted from Vourlitis and da Rocha (2010) using WebPlotDigitizer (Ankit, 2017). Additionally, Dalmagro 19 values represent averages for anaerobic (wet season) and aerobic (dry season) conditions over 2014 to 2017 rather than monthly averages. To align with the seasonal patterns in the Pantanal region, the anaerobic and aerobic period averages from Dalmagro et al. (2019) are represented in March and October, respectively. This assignment provides a general alignment with the typical timing of wet (anaerobic) and dry (aerobic) periods, although these values span varying dates each year. See Dalmagro et al. (2019) for full period definitions.

characterized by open arboreal woodland or closed forest (Vourlitis and da Rocha, 2010). The site had a mean annual temperature of 24 °C and precipitation of 2000 mm, which are approximately 9% and 35% higher than our site's conditions, respectively (Vourlitis et al., 2001). Vourlitis et al. (2001) found that the cerradão woodland's wet season (February, April) average daytime (0600–1800 h) NEE of CO_2 was -10 μmol m^{-2} s^{-1}, while the respective dry season (August–September) average was substantially lower at -2.3 μmol m^{-2} s^{-1} (Vourlitis et al., 2001). In comparison, the wooded Cerrado we studied exhibited a lower wet season average daytime NEE of CO_2 around -7.4 μmol m^{-2} s^{-1} but showed less seasonal variability and a higher dry season average daytime NEE of CO_2 around -5.4 μmol m^{-2} s^{-1}. The higher dry season carbon uptake at our site makes the wooded Cerrado a much stronger carbon sink. Compared to our site, a very similar wet season daytime CO_2 flux of -6.6 μmol m^{-2} s^{-1} was reported by Dalmagro et al. (2019) as a multi-annual average. At this seasonally flooded gallery forest site at the fringe of the Cerrado ecoregion, which was also studied by Vourlitis et al. (2022), average daytime CO_2 uptake rates during the dry season were, however, substantially lower (-2.7 μmol m^{-2} s^{-1}) than at our site. The average annual NEE-C uptake at this *mata galeria* forest was consequently a lot lower (230 g m^{-2} yr^{-1}) compared to our *Cerrado sensu stricto* site (541 ± 26 g m^{-2} yr^{-1}). This difference can be traced back to a slightly lower cumulative annual ecosystem respiration flux at our site (cumulative carbon exchange via ecosystem respiration in Vourlitis et al. (2022): 1410 g m^{-2} yr^{-1}, our study: 1337 ± 49 g m^{-2} yr^{-1}) while photosynthesis-related cumulative CO_2 uptake was larger at our site (cumulative carbon exchange via gross primary production in Vourlitis et al. (2022): −1630 g m^{-2} yr^{-1}, our study: −1880 ± 49 g m^{-2} yr^{-1}).

For the same site, Dalmagro et al. (2014) presented leaf scale measurements of carbon dioxide exchange of the two tree species dominating the investigated wetland forest, which both are not present at the site from which we report in the study at hand. From the leaf scale measurements, Dalmagro et al. (2014) inferred ecosystem functional parameters, similar to our approach, albeit on the ecosystem level in our case. Although differences arise between EFP time series inferred on different spatial scales, they are of similar magnitude between the two sites. In particular, while maximum photosynthesis at the Pantanal gallery forest is about half of the values reported here for the wooded Cerrado, initial quantum yield is about 50% lower at our site pointing towards light-limitation being more of an issue for trees at the gallery forest compared to the wooded Cerrado we report from here. The combination of plant adaptation to lower light conditions could point towards generally lower light availability at the gallery forest. This difference in environmental conditions might have contributed to the comparably larger annual gross photosynthetic uptake of CO_2 at our site.

In summary, contrary to previous studies, which suggested that the wooded Cerrado's wet season NEE-C uptake is balanced by dry season NEE-C release, our study, with the longest observation period among the studies, found that the wooded Cerrado can remain a strong carbon sink during the dry season. Consequently, it emerges as a much stronger carbon sink than previously observed. Its robust performance in NEE-C uptake during the dry season and throughout the year makes it more comparable to tropical forests than to savanna woodlands. This finding indicates that the wooded Cerrado's function as a carbon sink is highly conditional and can vary significantly. However, further study is needed to determine whether our findings are local or regional.

4.2. Comparison of the pasture to other grassland ecosystems

We compared the NEE-C uptake of the pasture with literature accounts of multiple planted forage pastures and a natural forage pasture across Brazil to put our results into perspective and further gain confidence in our modeling (especially the source partitioning) approach (Table 8). Firstly, we compared the pasture to a nearby *Brachiaria sp.* pasture at Três Lagoas, Mato Grosso do Sul state, Brazil (21° 0.9685' S) (Alves et al., 2021), and found that both sites exhibited similar annual NEE-C uptake. Specifically, Alves et al. (2021) measured the carbon uptake of a *Brachiaria sp.* pasture located approximately 440 km away from our site using the EC method from 2016 to 2018. The site has Oxisols with an annual precipitation of around 1300 to 1600 mm and an annual temperature of around 22 to 24 °C (Alves et al., 2021). Given that our pasture site shares the same dominant grass type, climate, and soil type, we expected its NEE-C uptake to be consistent with the Três Lagoas site. Alves et al. (2021) reported that the Três Lagoas pasture had an NEE-C uptake of −171.8 ±15.8 g m^{-2} yr^{-1} for the hydrological year 2017 to 2018. This value closely matches the highest NEE-C uptake of pasture that we observed, which was −179 ±38 g m^{-2} yr^{-1} in 2020. However, the Três Lagoas pasture reached −208.9 ±9.6 g m^{-2} yr^{-1} in the hydrological year 2016 to 2017, surpassing the highest annual NEE-C uptake observed at the pasture. This difference could be attributed to the active grazing at our pasture site, in contrast to the absence of active grazing at the Três Lagoas site (Alves et al., 2021). Additionally, the fact that our pasture site is mixed with a small segment of sugarcane field could also contribute to this difference.

Secondly, the NEE-C uptake of the pasture was lower when compared to cultivated pasture in Northeast Brazil. Bezerra et al. (2022) used the EC method to measure the NEE-C uptake of a *Brachiaria brizantha* pasture located in Rio Grande do Norte State, Northeast Brazil (5° 53.5667' S). While both sites exhibited similar annual precipitation, the Bezerra et al. (2022) site had a higher annual average temperature of 25.5 °C and a different soil type, which was classified as Entisol. Additionally, Bezerra et al. (2022) site was used for sheep grazing, in contrast to our site's cattle grazing. Under these varying conditions, the study found that the site had an average NEE-C uptake of −215 ±22 g m^{-2} yr^{-1} based on two years of measurements (Bezerra et al., 2022). In contrast, our pasture site had an average NEE-C uptake of −162.5 g m^{-2} yr^{-1}, which is about 24.4% lower than the site studied by Bezerra

Table 8
Comparison of pasture's annual NEE-C uptake with other literature.

Site	Active grazing	Study period	NEE-C g m^{-2} yr^{-1}
This study	Yes	2019	−146 ± 39
		2020	−179 ± 38
Alves et al. (2021)	No	2016 October to 2017 September	−208.9 ± 9.6
		2018 October to 2018 September	−171.8 ± 15.8
Bezerra et al. (2022)	Yes	2015 October to 2016 September	−199
		2016 October to 2017 September	−230
Roberti et al. (2024)	Yes	Average from 2015 to 2020	−207.6 ± 118.0

et al. (2022). This aligns with Bezerra et al. (2022)'s hypothesis that pastures in Northeast Brazil are stronger CO_2 sinks than those in Cerrado biomes. Bezerra et al. (2022) also found that the seasonality of a pasture's CO_2 uptake was strongly associated with changes in precipitation, which is consistent with our findings about the pasture.

Thirdly, we compared our pasture site with a natural pasture used for cattle grazing in the Brazilian Pampa biome, located in Rio Grande do Sul State (29° 43.4584' S) (Roberti et al., 2024). Compared to our site in the Cerrado biome, the climate of the site in the Pampa biome region is characterized by a lower mean annual temperature of 19.4 °C, a 20% higher mean annual precipitation of 1778 mm, and distinct seasons (Roberti et al., 2024). The natural pasture comprises "uniformly distributed" C4 grasses including *Axonopus affinis*, *Paspalum notatum*, *Andropogon lateralis*, and *Aristida laevisis* (Roberti et al., 2024). Roberti et al. (2024) found that the natural pasture is capable of achieving a mean annual NEE-C uptake of −207.6 ±118.0 g m^{-2} yr^{-1}, but with strong interannual variability. From 2015 to 2020, the annual NEE-C uptake value of the natural pasture site ranged from −82.0 to −385.3 g m^{-2} yr^{-1} (Roberti et al., 2024). In comparison, our site had a 28% lower mean annual NEE-C uptake and a lower interannual variability. However, as we only have two complete years of records, longer observation is needed to compare the interannual variability. Nevertheless, our pasture site exhibited a comparable NEE-C uptake to a natural pasture with lower interannual variability.

In summary, we found that the pasture functioned as a CO_2 sink, with a NEE-C uptake relatively lower than cultivated and natural pastures in other biomes of Brazil. Its seasonal variability in NEE-C is highly correlated with precipitation, which is consistent with other studies on cultivated pasture in Brazil (Bezerra et al., 2022; Alves et al., 2021). In addition, the comparison to other pasture sites showed that the estimated NEE-C of our site is within a reasonable range, but dedicated EC measurements or chamber measurements at the pasture are needed to further validate our results. Furthermore, due to the lack of grazing management records and additional environmental data, including soil properties and ET of the site, we could not pinpoint the cause of the lower NEE-C uptake at the pasture.

4.3. Two ecosystems' different response to precipitation variability

We found that the pasture site was more susceptible to changes in precipitation during the wet season than the wooded Cerrado, which is evident from the 1140 % higher SD in the total wet season NEE-C at the pasture site across three periods. In addition, the heavy rainfall event during P2's wet season (February 2020) (Fig. B.12(a)), which drove the high seasonal and inter-annual variability in precipitation throughout the study period, further revealed the pasture's vulnerability to sudden excessive rainfall. Specifically, during P2's wet season, the NEE-C uptake in the wooded Cerrado remained similar to that in P1's wet season, whereas the pasture's NEE-C uptake dropped by 83%. One contributing factor to this difference could be the predominance of grasses with shorter roots in the pasture. The heavy rainfall likely caused waterlogged conditions in the top soil layer, leading to the suffocation, decay, and death of the grassroots, which in turn reduced GPP-C (Nasrullah et al., 2022). Moreover, grazing activity at the pasture site causes soil compaction and lowers the infiltration rate (Centeri, 2022), potentially prolonging waterlogged conditions. In contrast, the wooded Cerrado is more resistant to waterlogged conditions in the topsoil with its deeper roots. Furthermore, the absence of grazing activity and the presence of perennial trees and a continuous shrub layer in the wooded Cerrado are associated with a higher infiltration rate, thus reducing the duration of waterlogging conditions (Eldridge and Freudenberger, 2005; Basche and DeLonge, 2019). Overall, our findings show the NEE-C of the wooded Cerrado at our site was less affected by the heavy rainfall event in the wet season than the pasture, possibly due to a combination of the factors outlined above.

Following the event, pasture's NEE-C started to recover during P2's dry season from April to August 2020. In P3's wet season, pasture's NEE-C returned to pre-event levels despite relatively low precipitation. We speculate that young grasses germinating after the event matured during P3's wet season, resulting in higher GPP-C and NEE-C for that period. Subsequently, during P3's dry season, precipitation dropped substantially compared to P2's and P1's dry seasons (Fig. B.12(a)). Despite this, the pasture achieved its highest dry season NEE-C uptake among the three dry seasons we investigated. Our results show that the *Brachiaria decumbens* in our pasture site can recover quickly from excessive rainfall and tolerate drought, similar to other perennial tropical forage grasses as reported by Baruch (1994) and Imaz et al. (2015).

On the other hand, the wooded Cerrado's total NEE-C remained mostly stable across the three periods, exhibiting higher variability than the pasture only in total dry season GPP-C. However, the wooded Cerrado can adjust its TER-C to maintain stable NEE-C throughout the three periods. The ET time series (Fig. B.12(b)) and high ET/P ratios (Fig. B.12(c)) during low precipitation periods also demonstrated both ecosystems' drought resilience. To better understand the drivers behind the annual variations in carbon fluxes for both sites, further investigation of environmental variables and human factors, including ET, vapor pressure deficit (VPD), soil water content, cloudiness, grazing activity, and others, is needed.

4.4. Impact of land-use change on carbon dioxide fluxes

Our findings revealed that converting wooded Cerrado into pasture resulted in a reduction in NEE-C uptake. The conversion to pasture caused a decrease in cumulative NEE-C uptake by 1084 g m^{-2} (58%) over the entire 35-month study period. Considering the annual NEE-C uptake, the transitioning led to a decrease in NEE-C uptake by up to 494 g m^{-2} yr^{-1} (73%). This conversion likely triggers a series of changes in local terrestrial hydrology and soil properties, which further influence carbon dynamics.

Moreover, the conversion intensifies the land's sensitivity to fluctuations in environmental variables, especially precipitation. The potential increase in extreme weather occurrences and more sporadic precipitation patterns in the future, due to climate change (Meehl et al., 2000), make the land's carbon uptake capability increasingly vulnerable and unpredictable. Implementing proper management, including irrigation and fertilization, could mitigate pasture's low dry season NEE-C and vulnerability to changes in precipitation. For example, Schipper et al. (2019) showed that irrigation could lower the soil respiration of pasture. Studies including de Freitas et al. (2020) and Santos et al. (2004) also found that proper management could increase pasture's NEE-C

uptake and soil carbon stock. However, estimating the overall effect of conversion-induced changes in the water cycle, soil properties, and carbon stock on the vegetation–climate feedback loop, and their subsequent impact on carbon uptake of the land, remains a significant challenge.

5. Conclusion

In this study, we experimented with three NEE partitioning models, including CPM-F, CPM-WD, and CPM-FS. We found that the CPM-F approach provided a convenient way to model the NEE-C of two sources and additionally partition them into GPP-C and TER-C. By comparing the modeled NEE-C for both ecosystems with the measured NEE-C found in other literature, we found that our model results are comparable and exhibited similar environmental response behavior.

The model results presented here show that, on a multi-annual data basis, wooded Cerrado is a stronger carbon sink compared to the pasture with planted *Brachiaria decumbens*. The conversion of wooded Cerrado to pasture led to a substantial reduction in NEE-C uptake. Although pasture can match wooded Cerrado's carbon uptake rate during the wet season, wooded Cerrado maintains higher dry season NEE-C uptake, resulting in an overall higher annual NEE-C uptake. Furthermore, pasture was found to be more sensitive to changes in precipitation, displaying more pronounced seasonal and periodic variations than wooded Cerrado. We propose that LULCC alters the infiltration rate and other soil properties of pasture, leading to a greater impact of precipitation on it. However, this theory requires further in-situ measurements for validation. Nonetheless, our study provides insights into the implications of converting wooded Cerrado into pasture and the potential causes of these effects. The data produced by our study lays a foundation for future research on the relationship between carbon flux, land management, and environmental drivers in these ecosystems.

CRediT authorship contribution statement

Yuqing Zhao: Writing – review & editing, Writing – original draft, Visualization, Software, Methodology, Formal analysis, Data curation. **David Holl:** Writing – review & editing, Supervision, Software, Methodology, Funding acquisition, Conceptualization. **Jamil A.A. Anache:** Writing – review & editing, Supervision, Project administration, Methodology, Investigation, Funding acquisition, Data curation, Conceptualization. **Alex N.A. Kobayashi:** Software, Formal analysis. **Edson Wendland:** Resources, Project administration, Investigation, Funding acquisition, Conceptualization.

Declaration of competing interest

The authors declare that they have no known competing financial interests or personal relationships that could have appeared to influence the work reported in this paper.

Acknowledgments

The authors acknowledge the Green Talents Program of the German Federal Ministry of Education and Research (BMBF) for the seed funding that allowed this research cooperation. This study was financially supported by the Brazilian Coordination for the Improvement of Higher Education Personnel (CAPES, Finance Code 001), the Brazilian National Council for Scientific and Technological Development (CNPQ, grant number 408997/2021-4) and the São Paulo Research Foundation (FAPESP, grant number 2015/03806–1). Lastly, the authors would like to acknowledge the Arruda Botelho Institute (IAB) for facilitating the study area and installations at the São José farm in Itirapina, São Paulo.

Appendix A. Calculation of model performance metrics

We assessed model performance by calculating Akaike's information criterion (AIC), mean squared error (MSE), bias error (BE), coefficient of determination (r^2), and root mean squared error (RMSE) using the following equations:

$$MSE = \frac{1}{n}\sum_{i=1}^{n}(m_i - o_i)^2 \tag{A.1}$$

$$AIC = n \times \ln(MSE) + 2 \times P_{\text{free}} \tag{A.2}$$

$$BE = \frac{1}{n}\sum_{i=1}^{n}(m_i - o_i) \tag{A.3}$$

$$r^2 = \left(\frac{\sum_{i=1}^{n}(m_i - \bar{m})(o_i - \bar{o})}{\sqrt{\sum_{i=1}^{n}(m_i - \bar{m})^2 \sum_{i=1}^{n}(o_i - \bar{o})^2}} \right)^2 \tag{A.4}$$

$$RMSE = \sqrt{\frac{\sum_{i=1}^{n}(m_i - o_i)^2}{n}} \tag{A.5}$$

Specifically, we first calculated the MSE by taking the mean of the squares of the differences between the observed NEE values (o_i) and modeled NEE values (m_i) using Eq. (A.1) (Hodson et al., 2021; Holl, 2017). With MSE values, AIC was calculated using Eq. (A.2) with the number of measured values (n), and the number of parameters in the model (P_{free}) (Holl, 2017). Additionally, BE was calculated similarly to MSE, but without taking the square root, as per Eq. (A.3) (Holl, 2017). r^2 and RMSE were calculated using Eq. (A.4) and Eq. (A.5), respectively (Holl, 2017). Here $\bar{m}$ and $\bar{o}$ represent the mean of the modeled values and the mean of the observed values, respectively.

Appendix B. Environmental and flux measurement conditions

See Figs. B.11–B.13.

Appendix C. Temporal CO_2 flux data distribution

See Figs. C.14 and C.15.

Appendix D. Double mass analysis of precipitation data

See Fig. D.16.

Appendix E. Time window selection for component partitioning models

See Figs. E.17–E.20.

Appendix F. Time series of EFPs

See Figs. F.21–F.24.

Data availability

Access the BR-IAB site description at https://ameriflux.lbl.gov/sites/siteinfo/BR-IAB (AmeriFlux, 2024). The dataset from BR-IAB can be found at https://doi.org/10.5281/zenodo.13912437 (Anache et al., 2024a). The results from this study on the BR-IAB are available at https://doi.org/10.5281/zenodo.12528643 (Zhao et al., 2024). The precipitation record for the BR-IAB is available at https://doi.org/10.5281/zenodo.11123751 (Anache et al., 2024b).

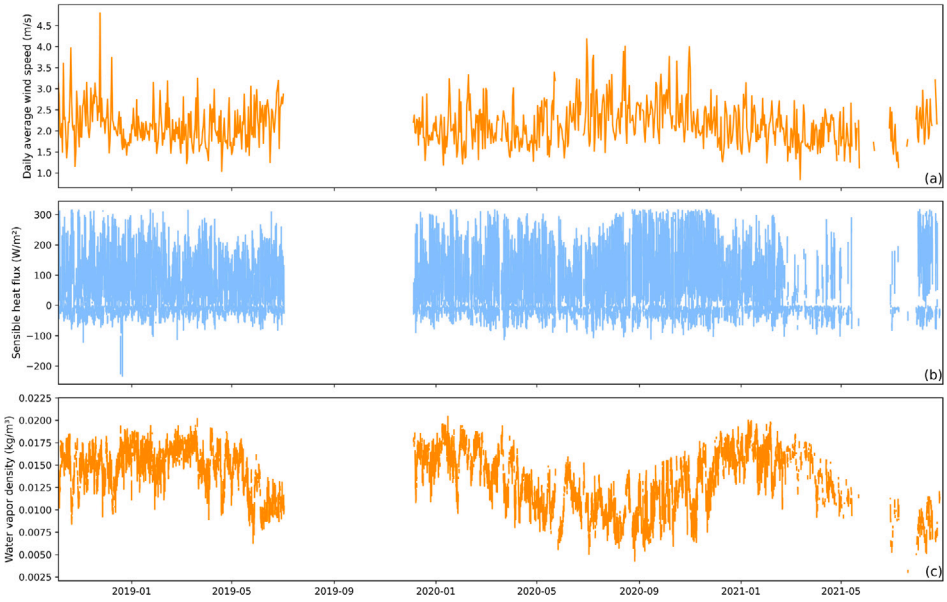

Fig. B.11. Environmental and flux measurement conditions throughout the study period, including (a) daily average wind speed (m/s), (b) half-hourly sensible heat flux (H) (W/m^2), (c) half-hourly water vapor density (kg/m^3), Half-hourly wind speed, H, and water vapor density data are filtered to include only instances where quality-filtered CO_2 flux data are available.

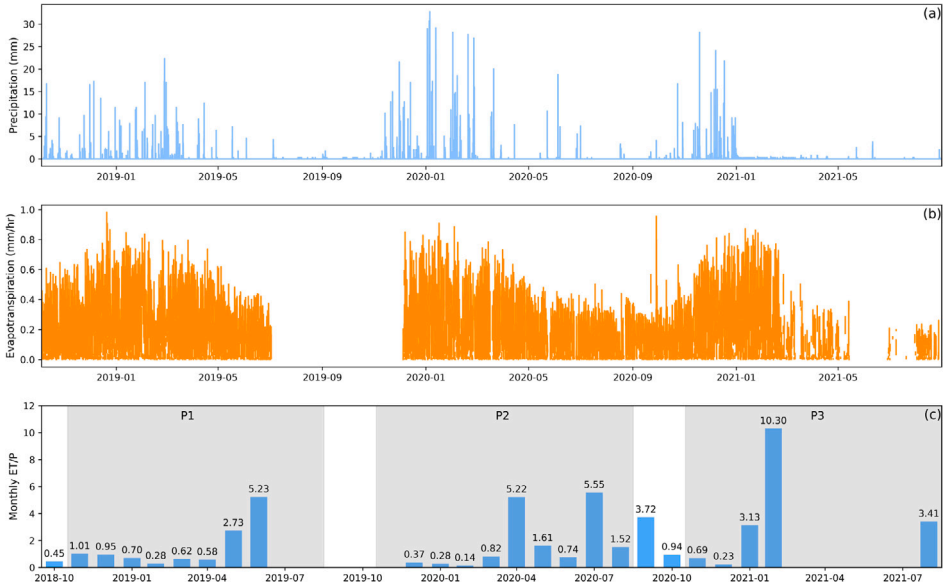

Fig. B.12. Hydrological parameters measured and calculated throughout the study period, including (a) half-hourly gap-filled precipitation (P) (mm), (b) half-hourly evapotranspiration (ET) (mm/hr), and (c) ratio of monthly cumulative ET to P (ET/P) with gray-shaded backgrounds marking three equal periods (P1: 2018-11-01 to 2019-08-31, P2: 2019-11-01 to 2020-08-31, P3: 2020-11-01 to 2021-08-31). All three parameters are processed using the method mentioned in Section 3.2.

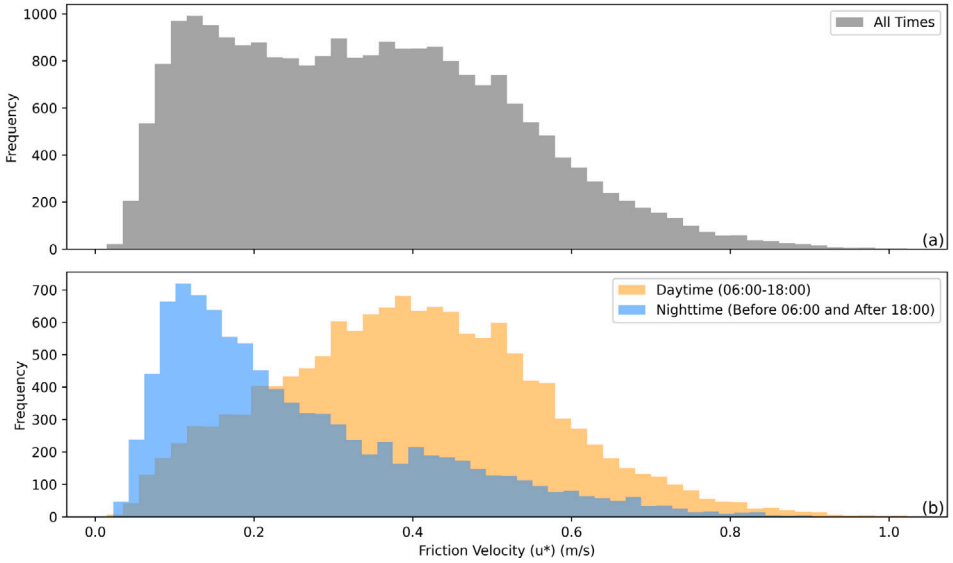

Fig. B.13. Histogram of friction velocity (u*, m/s) values corresponding to quality filtered CO_2 flux data (see Section 3.1). Plot (a) shows the overall distribution of u* values across all times, while plot (b) separates the u* into daytime (06:00–18:00, in orange) and nighttime (before 06:00 and after 18:00, in blue) periods, which highlights the distribution of u* values during different times of the day. The difference in u* distribution reflects variations in atmospheric turbulence during the day–night cycle, which directly impacts the quality of CO_2 flux measurements. Lower u* values at night are typical due to more stable atmospheric conditions with reduced turbulence, which can lead to insufficient gas mixing and underestimation of CO_2 fluxes. In contrast, higher daytime u* values indicate enhanced turbulence from solar heating, which facilitates effective gas transport and improves CO_2 flux measurement accuracy.

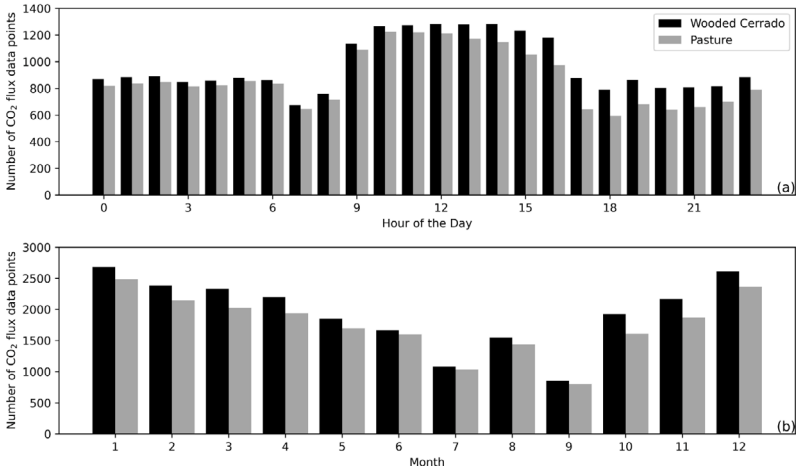

Fig. C.14. Number CO_2 flux data points after quality filtering with non-zero contributions to the eddy covariance footprint from the wooded Cerrado and pasture, grouped by hour of the day (a) and month (b).

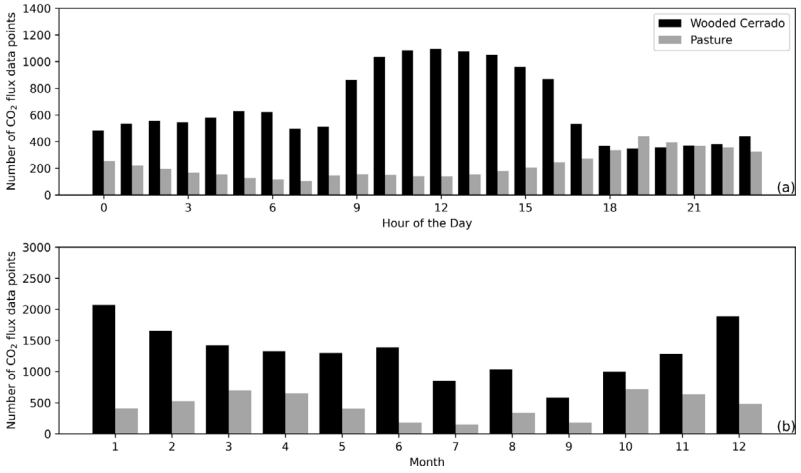

Fig. C.15. Number of CO_2 flux data points based on wind direction division for wooded Cerrado and pasture, grouped by hour of the day (a) and month (b).

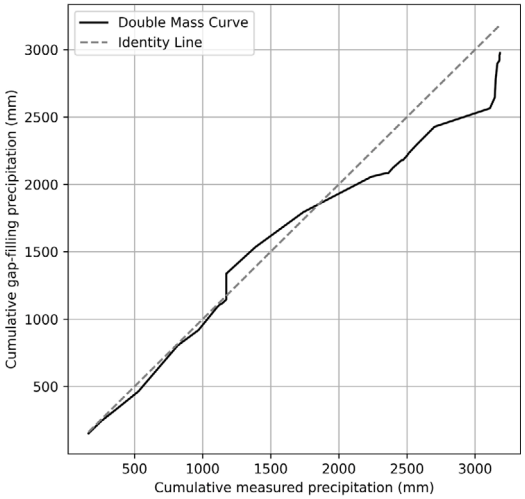

Fig. D.16. Double mass curve comparing gap-filling and measured precipitation data. The black line represents the cumulative sums of measured precipitation plotted against the cumulative sums of gap-filling precipitation data. The gray dashed line is the identity line.

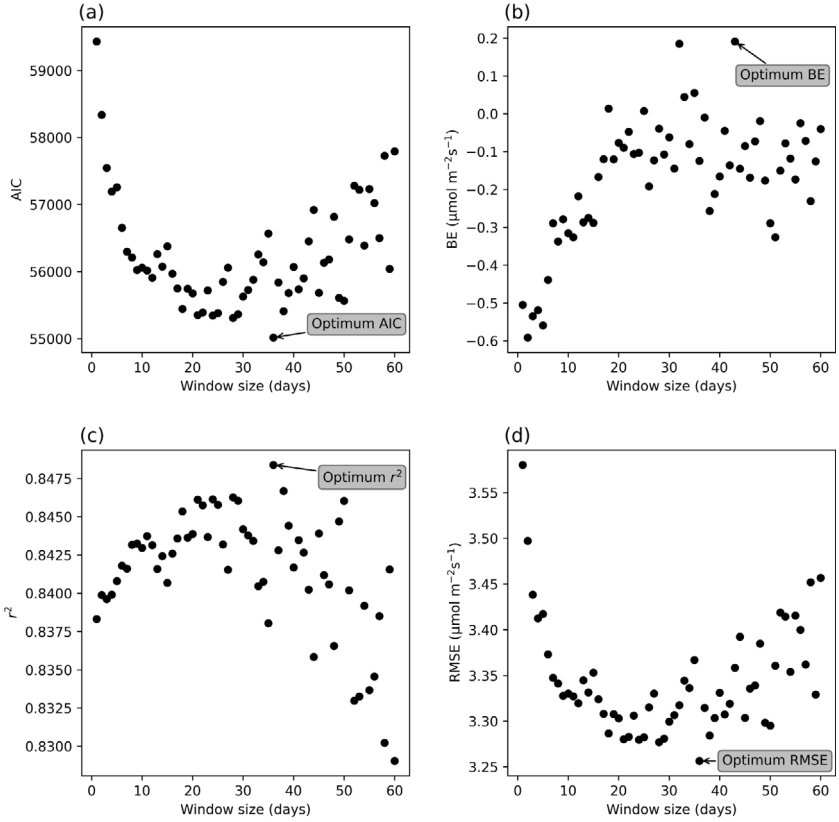

Fig. E.17. Correlation between time window sizes used for estimating ecosystem functional properties (EFP) in the component partitioning model (CPM) and model performance metrics, including AIC (a), BE (b), r^2 (c), and RMSE (d).

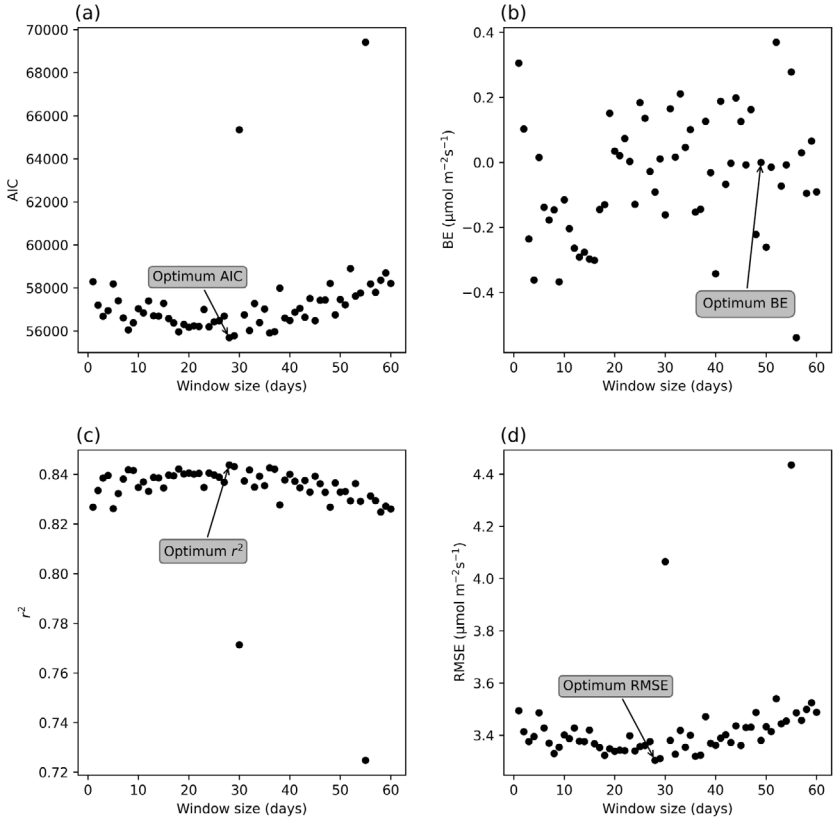

Fig. E.18. Correlation between time window sizes used for estimating EFPs in the component partitioning model with flux footprint-based source partitioning (CPM-F) and model performance metrics, including AIC (a), BE (b), r^2 (c), and RMSE (d).

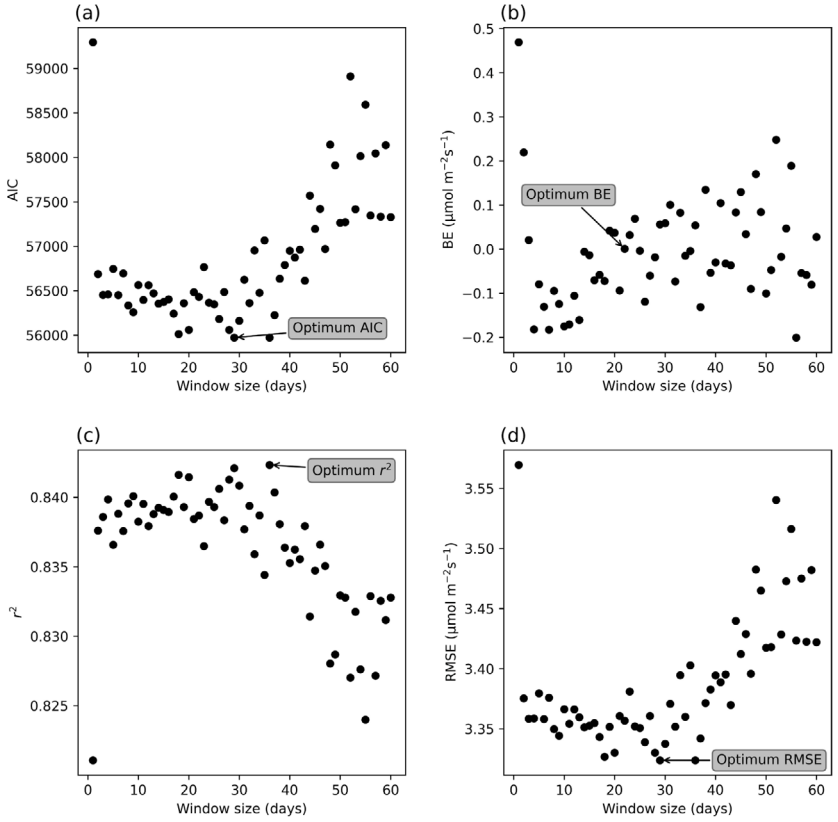

Fig. E.19. Correlation between time window sizes used for estimating EFPs in the stepwise component partitioning model with flux footprint-based source partitioning (CPM-FS) and model performance metrics, including AIC (a), BE (b), r^2 (c), and RMSE (d).

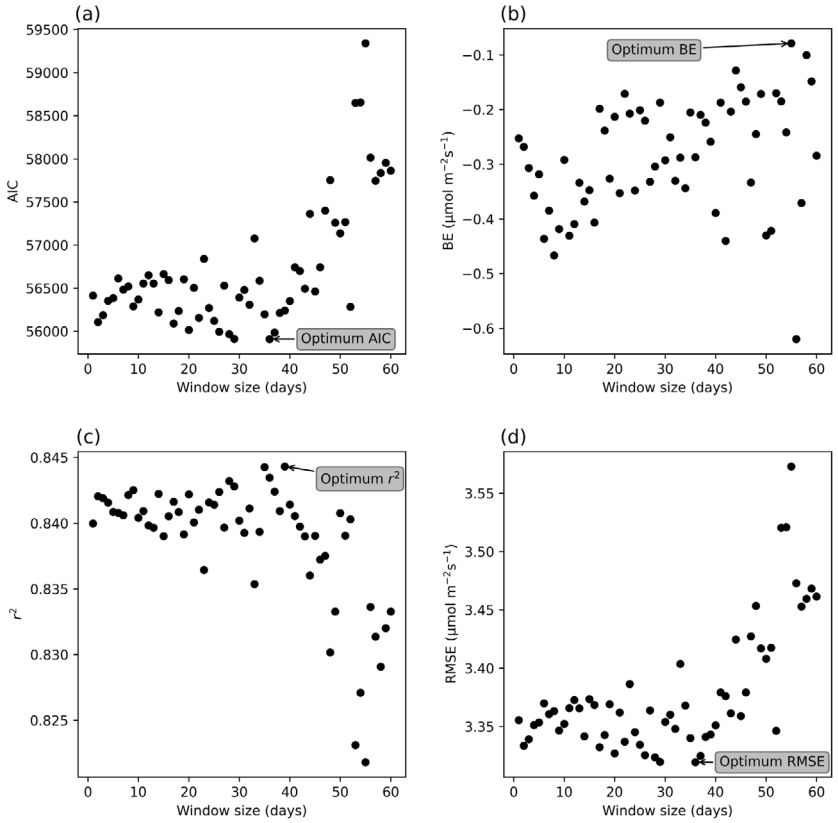

Fig. E.20. Correlation between time window sizes used for estimating EFPs in the component partitioning model with wind direction-based source partitioning (CPM-WD) and model performance metrics, including AIC (a), BE (b), r^2 (c), and RMSE (d).

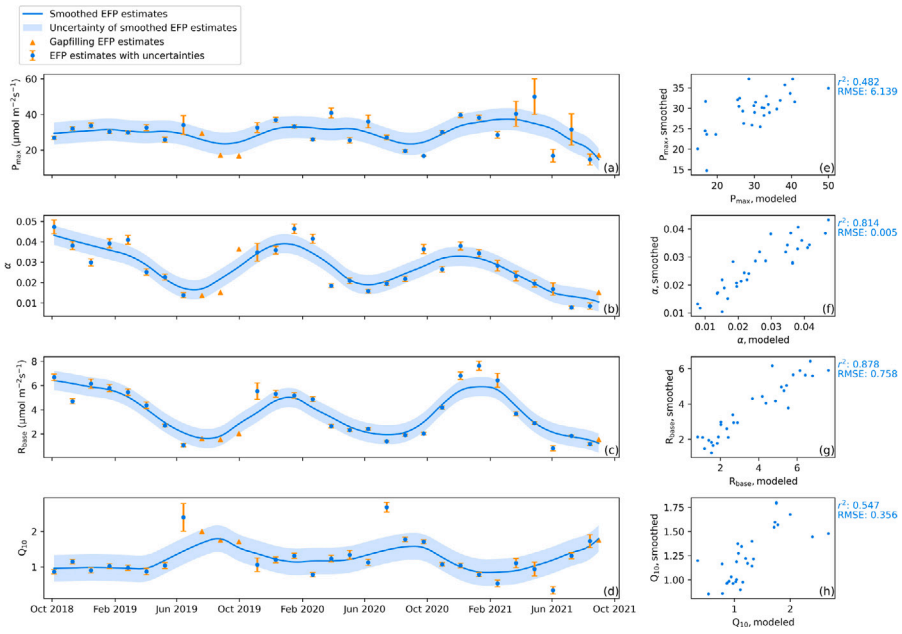

Fig. F.21. Gap-filled and smoothed time series of EFP estimates, including maximum photosynthesis P_{max} (a), initial quantum yield α (b), base respiration R_{base} (c), and temperature sensitivity coefficient Q_{10} (d) using CPM. Panels (e) to (h) show the linear regression between the raw EFP estimates and the LOWESS smoothed EFP estimates, with r^2 and RMSE values. Blue dots with error bars represent raw EFP estimates with a 68% confidence interval (CI); orange triangles denote gap-filling EFP estimates obtained by averaging the corresponding EFP estimates from the same month in other years; the blue line with shaded areas around it shows locally weighted regression (LOWESS) smoothed EFP estimates with a 95% CI.

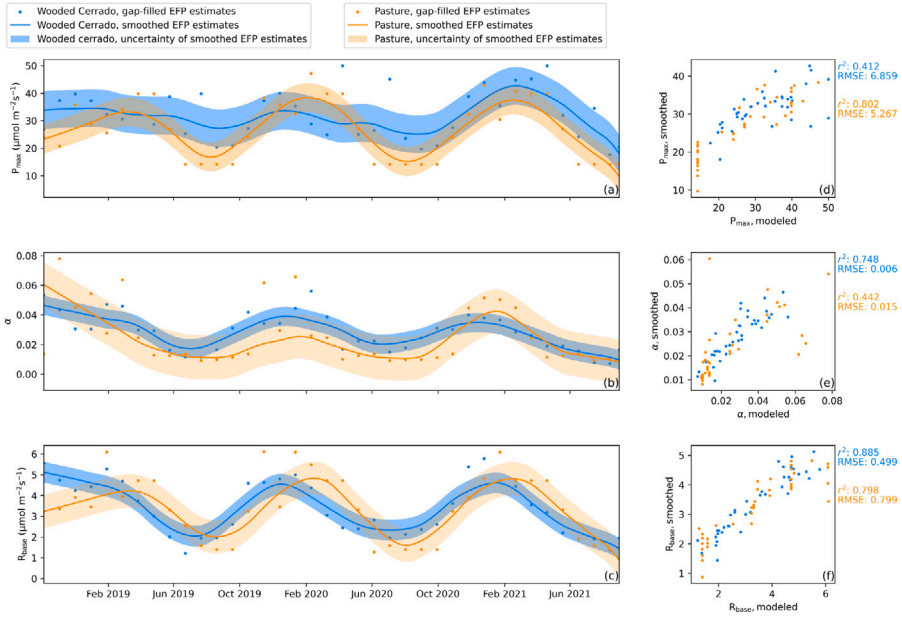

Fig. F.22. Gap-filled and smoothed time series of EFP estimates, including P_{max} (a), α (b), and R_{base} (c) using CPM-F for both ecosystems. Panels (d) to (f) show the linear regression between the raw EFP estimates and the LOWESS smoothed EFP estimates, with r^2 and RMSE values. Dots represent gap-filled EFP estimates, while lines with shaded areas around them show LOWESS smoothed EFP estimates with a 95% CI.

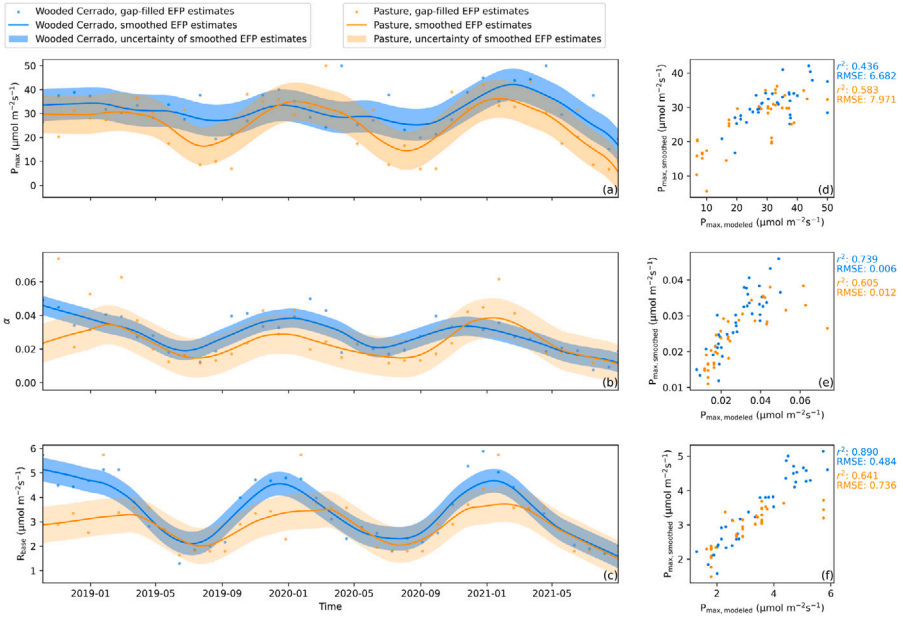

Fig. F.23. Gap-filled and smoothed time series of EFP estimates, including P_{max} (a), α (b), and R_{base} (c) using CPM-FS for both ecosystems. Panels (d) to (f) show the linear regression between the raw EFP estimates and the LOWESS smoothed EFP estimates, with r^2 and RMSE values. Dots represent gap-filled EFP estimates, while lines with shaded areas around them show LOWESS smoothed EFP estimates with a 95% CI.

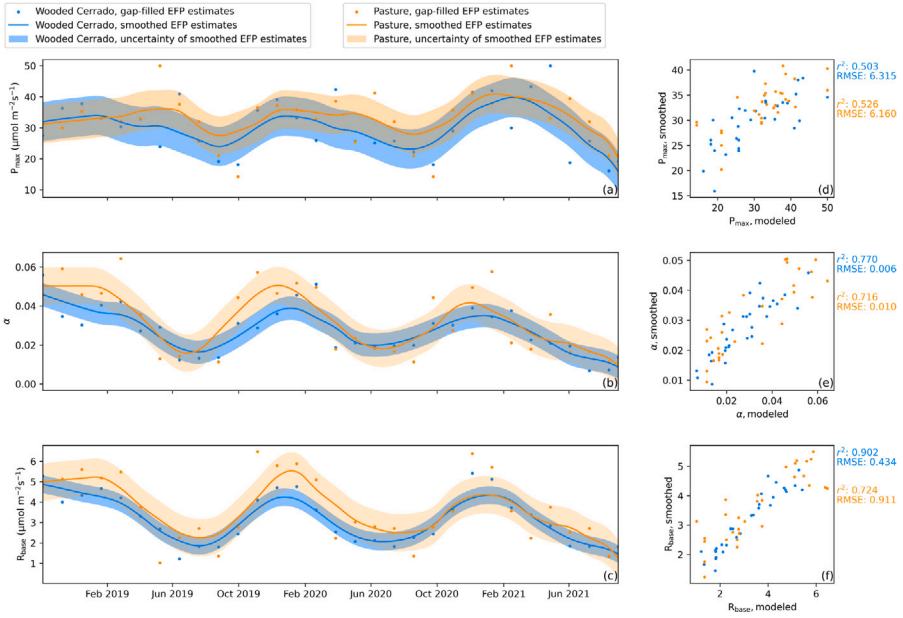

Fig. F.24. Gap-filled and smoothed time series of EFP estimates, including P_{max} (a), α (b), and R_{base} (c) using CPM-WD for both ecosystems. Panels (d) to (f) show the linear regression between the raw EFP estimates and the LOWESS smoothed EFP estimates, with r^2 and RMSE values. Dots represent gap-filled EFP estimates, while lines with shaded areas around them show LOWESS smoothed EFP estimates with a 95% CI.

References

Alberton, B., Almeida, J., Helm, R., da S. Torres, R., Menzel, A., Cerdeira Morellato, L.P., 2014. Using phenological cameras to track the green up in a cerrado savanna and its on-the-ground validation. Ecol. Informatics 19, 62–70. http://dx.doi.org/10.1016/j.ecoinf.2013.12.011, URL https://www.sciencedirect.com/science/article/pii/S1574954113001325.

Alves, J.D.N., Ribeiro, A., Rody, Y.P., Loos, R.A., Hall, K.B., 2021. Carbon uptake and water vapor exchange in a pasture site in the Brazilian Cerrado. J. Hydrol. 594, 125943. http://dx.doi.org/10.1016/j.jhydrol.2020.125943, URL https://www.sciencedirect.com/science/article/pii/S0022169420314049.

AmeriFlux, 2024. AmeriFlux Site Info: BR-IAB. URL https://ameriflux.lbl.gov/sites/siteinfo/BR-IAB, Accessed: 2024-06-29.

Anache, J.A.A., Kobayashi, A.N.A., Wendland, E., 2024a. Eddy covariance dataset for BR-IAB: Instituto Arruda Botelho - Wooded Cerrado and Mixed Agriculture. http://dx.doi.org/10.5281/zenodo.13912437, URL https://zenodo.org/uploads/13912437, [dataset].

Anache, J.A.A., Wendland, E., Rosalem, L.M.P., Youlton, C., Oliveira, P.T.S., 2019. Hydrological trade-offs due to different land covers and land uses in the Brazilian Cerrado. Hydrol. Earth Syst. Sci. 23, 1263–1279. http://dx.doi.org/10.5194/hess-23-1263-2019, URL https://hess.copernicus.org/articles/23/1263/2019/.

Anache, J.A.A., Zhao, Y., Holl, D., Wendland, E., 2024b. 5-minute precipitation data in itirapina, Brazil (2015–2022). http://dx.doi.org/10.5281/zenodo.11123751, [dataset].

Andrade, A.S., Santos, P.M., Pezzopane, J.R.M., de Araujo, L.C., Pedreira, B.C., Pedreira, C.G.S., Marin, F.R., Lara, M.A.S., 2016. Simulating tropical forage growth and biomass accumulation: an overview of model development and application. Grass Forage Sci. 71 (1), 54–65. http://dx.doi.org/10.1111/gfs.12177, URL https://onlinelibrary.wiley.com/doi/abs/10.1111/gfs.12177.

Ankit, R., 2017. WebPlotDigitizer. URL https://automeris.io/wpd/, Version 5 [software].
Arruda, P.H.Z., Vourlitis, G.L., Santanna, F.B., Pinto Jr., O.B., Lobo, F.A., Nogueira, J.S., 2016. Large net CO2 loss from a grass-dominated tropical savanna in south-central Brazil in response to seasonal and interannual drought. J. Geophys. Res.: Biogeosci. 121 (8), 2110–2124. http://dx.doi.org/10.1002/2016JG003404, URL https://agupubs.onlinelibrary.wiley.com/doi/abs/10.1002/2016JG003404.
Baruch, Z., 1994. Responses to drought and flooding in tropical forage grasses. Plant Soil 164, 87–96. http://dx.doi.org/10.1007/BF00010114.
Basche, A.D., DeLonge, M.S., 2019. Comparing infiltration rates in soils managed with conventional and alternative farming methods: A meta-analysis. PLOS ONE 14 (9), 1–22. http://dx.doi.org/10.1371/journal.pone.0215702.
Batista, D.S., Norat, J., 2019. Deforestation in Brazil's Cerrado. Technical Report, Map the System, University of Oxford.
Batlle-Bayer, L., Batjes, N.H., Bindraban, P.S., 2010. Changes in organic carbon stocks upon land use conversion in the Brazilian Cerrado: A review. Agricult. Ecosys. Environ. 137, 47–58. http://dx.doi.org/10.1016/j.agee.2010.02.003, URL https://linkinghub.elsevier.com/retrieve/pii/S016788091000037X.
Bezerra, B.G., Santos e Silva, C.M., Mendes, K.R., Mutti, P.R., Fernandes, L.S., Marques, T.V., Câmara e Silva, C.L., Campos, S., de Lima Vieira, M.M., Urbano, S.A., Difante, G.S., Ferreira, R.R., da Silva, D.T.C., Costa, G.B., Oliveira, P.E.S., de Oliveira, C.P., Gonçalves, W.A., Lucio, P.S., 2022. CO2 exchanges and evapotranspiration of a grazed pasture under tropical climate conditions. Agricult. Forest. Meterol. 323, 109088. http://dx.doi.org/10.1016/j.agrformet.2022.109088, URL https://www.sciencedirect.com/science/article/pii/S0168192322002763.
Britton, C.M., Dodd, J.D., 1976. Relationships of photosynthetically active radiation and shortwave irradiance. Agric. Meteorol. 17 (1), 1–7. http://dx.doi.org/10.1016/0002-1571(76)90080-7, URL https://www.sciencedirect.com/science/article/pii/0002157176900807.
Burton, J.A., 1985. The value of conserving genetic resources. Oryx 19 (1), 55. http://dx.doi.org/10.1017/S0030605300019670.
Carvalho, F.A., Hugo, V., Rodrigues, P., Kilca, R., Siqueira, A., Araújo, G., Schiavini, I., 2008. Composição florística, riqueza e diversidade de um cerrado Sensu stricto no sudeste do estado de Goiás. Biosci. J. 24, 64–72, URL https://seer.ufu.br/index.php/biosciencejournal/article/view/6769.
Carvalho, J.L.N., Raucci, G.S., Cerri, C.E.P., Bernoux, M., Feigl, B.J., Wruck, F.J., Cerri, C.C., 2010. Impact of pasture, agriculture and crop-livestock systems on soil C stocks in Brazil. Soil Tillage Res. 110, 175–186. http://dx.doi.org/10.1016/j.still.2010.07.011, URL https://linkinghub.elsevier.com/retrieve/pii/S0167198710001364.
Centeri, C., 2022. Effects of grazing on water erosion, compaction and infiltration on grasslands. Hydrology 9, 34. http://dx.doi.org/10.3390/hydrology9020034, URL https://www.mdpi.com/2306-5338/9/2/34.
Cleveland, W.S., Devlin, S.J., 1988. Locally weighted regression: An approach to regression analysis by local fitting. J. Amer. Statist. Assoc. 83, 596–610. http://dx.doi.org/10.1080/01621459.1988.10478639, URL https://www.tandfonline.com/doi/abs/10.1080/01621459.1988.10478639.
Cunha, A.P.M.A., Alvalá, R.C.S., Kubota, P.Y., Vieira, R.M.S.P., 2015. Impacts of land use and land cover changes on the climate over Northeast Brazil. Atmos. Sci. Lett. 16, 219–227. http://dx.doi.org/10.1002/ASL2.543, URL https://rmets.onlinelibrary.wiley.com/doi/abs/10.1002/asl2.543.
da Rocha, H.R., Freitas, H.C., Rosolem, R., Juárez, R.I.N., Tannus, R.N., Ligo, M.A., Cabral, O.M.R., Silva Dias, M.A.F., 2002. Measurements of CO2 exchange over a woodland savanna (Cerrado Sensu stricto) in southeast Brasil. Biota Neotrop. 2, 1–11. http://dx.doi.org/10.1590/S1676-06032002000100009, URL http://www.scielo.br/scielo.php?script=sci_arttext&pid=S1676-06032002000100009&lng=en&tlng=en.
Dalmagro, H.J., Lobo, F.A., Vourlitis, G.L., Dalmolin, A.C., Antunes, M.Z., Ortíz, C.E.R., Nogueira, J.S., 2014. The physiological light response of two tree species across a hydrologic gradient in Brazilian savanna (Cerrado). Photosynthetica 52 (1), 22–35. http://dx.doi.org/10.1007/s11099-014-0001-5.
Dalmagro, H.J., Zanella de Arruda, P.H., Vourlitis, G.L., Lathuillière, M.J., Nogueira, J.S., Couto, E.G., Johnson, M.S., 2019. Radiative forcing of methane fluxes offsets net carbon dioxide uptake for a tropical flooded forest. Global Change Biol. 25 (6), 1967–1981. http://dx.doi.org/10.1111/gcb.14615, URL https://onlinelibrary.wiley.com/doi/abs/10.1111/gcb.14615.
de Freitas, I.C., Ribeiro, J.M., Araújo, N.C.A., Santos, M.V., Sampaio, R.A., Fernandes, L.A., Azevedo, A.M., Feigl, B.J., Cerri, C.E.P., Frazão, L.A., 2020. Agrosilvopastoral systems and well-managed pastures increase soil carbon stocks in the Brazilian cerrado. Rangel. Ecol. Manag. 73 (6), 776–785. http://dx.doi.org/10.1016/j.rama.2020.08.001, URL https://www.sciencedirect.com/science/article/pii/S155074242030083X.
Didan, K., 2021. MODIS/Terra vegetation indices 16-day L3 global 250 m SIN grid V061. http://dx.doi.org/10.5067/MODIS/MOD13Q1.061, [dataset].
Dijk, A.v., 2002. Extension to 3D of "The Effect of Line Averaging on Scalar Flux Measurements with a Sonic Anemometer near the Surface" by Kristensen and Fitzjarrald. J. Atmos. Ocean. Technol. 19, 80–82. http://dx.doi.org/10.1175/1520-0426(2002)019<0080:ETOTEO>2.0.CO;2.
Eldridge, D.J., Freudenberger, D., 2005. Ecosystem wicks: Woodland trees enhance water infiltration in a fragmented agricultural landscape in eastern Australia. Austral Ecol. 30 (3), 336–347. http://dx.doi.org/10.1111/j.1442-9993.2005.01478.x, URL https://onlinelibrary.wiley.com/doi/abs/10.1111/j.1442-9993.2005.01478.x.
Felfili, J.M., da Silva, M.C., 1993. A comparative study of cerrado (sensu stricto) vegetation in central Brazil. J. Trop. Ecol. 9 (3), 277–289, URL http://www.jstor.org/stable/2559525.
Foken, T., Leuning, R., Oncley, S.R., Mauder, M., Aubinet, M., 2012. Eddy Covariance: A Practical Guide to Measurement and Data Analysis. Springer Netherlands, Dordrecht, pp. 85–131. http://dx.doi.org/10.1007/978-94-007-2351-1.
Forbrich, I., Kutzbach, L., Wille, C., Becker, T., Wu, J., Wilmking, M., 2011. Cross-evaluation of measurements of peatland methane emissions on microform and ecosystem scales using high-resolution landcover classification and source weight modelling. Agricult. Forest. Meterol. 151, 864–874. http://dx.doi.org/10.1016/j.agrformet.2011.02.006, URL https://www.sciencedirect.com/science/article/pii/S016819231100058X.
Goodland, R., 1971. A physiognomic analysis of the 'cerrado' vegetation of central brasil. J. Ecol. 59 (2), 411–419. http://dx.doi.org/10.2307/2258321, URL http://www.jstor.org/stable/2258321.
Gorgone Barbosa, E., Pivello, V.R., Meirelles, S.T., 2008. Allelopathic evidence in brachiaria decumbens and its potential to invade the Brazilian Cerrados. Braz. Arch. Biol. Technol. 51, 625–631. http://dx.doi.org/10.1590/S1516-89132008000400021, URL https://www.researchgate.net/publication/237564672_Allelopathic_evidence_in_Brachiaria_decumbens_and_its_potential_to_invade_the_Brazilian_Cerrados.
Hartemink, A.E., Zhang, Y., Bockheim, J.G., Curi, N., Silva, S.H.G., Grauer-Gray, J., Lowe, D.J., Krasilnikov, P., 2020. Chapter three - soil horizon variation: A review. In: Advances in Agronomy, Vol. 160, Academic Press, pp. 125–185. http://dx.doi.org/10.1016/bs.agron.2019.10.003, URL https://www.sciencedirect.com/science/article/pii/S0065211319301087.
Heuzé, V., Tran, G., Boval, M., Lebas, F., 2021. Signal grass (Brachiaria decumbens). URL https://www.feedipedia.org/node/489.
Hodson, T.O., Over, T.M., Foks, S.S., 2021. Mean squared error, deconstructed. J. Adv. Model. Earth Syst. 13 (12), http://dx.doi.org/10.1029/2021MS002681, e2021MS002681, URL https://agupubs.onlinelibrary.wiley.com/doi/abs/10.1029/2021MS002681.
Holl, D., 2017. Carbon Dioxide and Methane Balances of Pristine and Degraded Temperate Peatlands: Empirical Modeling of Eddy Covariance Trace Gas Fluxes Measured Over Heterogeneous Terrain (Ph.D. thesis). Universität Hamburg, URL https://ediss.sub.uni-hamburg.de/handle/ediss/7247.
Holl, D., Pancotto, V., Heger, A., Camargo, S.J., Kutzbach, L., 2019a. Cushion bogs are stronger carbon dioxide net sinks than moss-dominated bogs as revealed by eddy covariance measurements on Tierra del Fuego, Argentina. Biogeosciences 16, 3397–3423. http://dx.doi.org/10.5194/bg-16-3397-2019, URL https://bg.copernicus.org/articles/16/3397/2019/.
Holl, D., Pfeiffer, E.-M., Kutzbach, L., 2020. Comparison of eddy covariance CO2 and CH4 fluxes from mined and recently rewetted sections in a northwestern German cutover bog. Biogeosciences 17, 2853–2874. http://dx.doi.org/10.5194/bg-17-2853-2020, URL https://bg.copernicus.org/articles/17/2853/2020/.
Holl, D., Wille, C., Sachs, T., Schreiber, P., Runkle, B.R.K., Beckebanze, L., Langer, M., Boike, J., Pfeiffer, E.-M., Fedorova, I., Bolshianov, D.Y., Grigoriev, M.N., Kutzbach, L., 2019b. A long-term (2002 to 2017) record of closed-path and open-path eddy covariance CO2 net ecosystem exchange fluxes from the Siberian Arctic. Earth Syst. Sci. Data 11 (1), 221–240. http://dx.doi.org/10.5194/essd-11-221-2019, URL https://essd.copernicus.org/articles/11/221/2019/.
Horst, T.W., Lenschow, D.H., 2009. Attenuation of scalar fluxes measured with spatially-displaced sensors. Bound.-Layer Meteorol. 130, 275–300. http://dx.doi.org/10.1007/s10546-008-9348-0.
Imaz, J.A., Giménez, D.O., Grimoldi, A.A., Striker, G.G., 2015. Ability to recover overrides the negative effects of flooding on growth of tropical grasses Chloris gayana and Panicum coloratum. Crop. Pasture Sci. 66, 100. http://dx.doi.org/10.1071/CP14172.
Jammet, M., Crill, P., Dengel, S., Friborg, T., 2015. Large methane emissions from a subarctic lake during spring thaw: Mechanisms and landscape significance. J. Geophys. Res.: Biogeosci. 120 (11), 2289–2305. http://dx.doi.org/10.1002/2015JG003137, URL https://agupubs.onlinelibrary.wiley.com/doi/abs/10.1002/2015JG003137.
Kaimal, J.C., Clifford, S.F., Lataitis, R.J., 1989. Effect of finite sampling on atmospheric spectra. Bound.-Layer Meteorol. 47, 337–347. http://dx.doi.org/10.1007/BF00122338.
Klink, C., Machado, R., 2005. Conservation of the Brazilian Cerrado. Conserv. Biol. 19 (3), 707–713. http://dx.doi.org/10.1111/j.1523-1739.2005.00702.x, URL https://conbio.onlinelibrary.wiley.com/doi/abs/10.1111/j.1523-1739.2005.00702.x.
Kljun, N., Calanca, P., Rotach, M.W., Schmid, H.P., 2015. A simple two-dimensional parameterisation for flux footprint prediction (FFP). Geosci. Model. Dev. 8, 3695–3713. http://dx.doi.org/10.5194/gmd-8-3695-2015, URL https://gmd.copernicus.org/articles/8/3695/2015/.
Kormann, R., Meixner, F.X., 2001. An analytical footprint model for non-neutral stratification. Bound.-Layer Meteorol. 99 (2), 207–224. http://dx.doi.org/10.1023/A:1018991015119.
Kutzbach, L., Wille, C., Pfeiffer, E.-M., 2007. The exchange of carbon dioxide between wet arctic tundra and the atmosphere at the Lena River Delta, Northern Siberia. Biogeosciences 4, 869–890. http://dx.doi.org/10.5194/bg-4-869-2007, URL https://bg.copernicus.org/articles/4/869/2007/.

Li, R., Wang, D., Wang, W., Nemani, R., 2023. A GeoNEX-based high-spatiotemporal-resolution product of land surface downward shortwave radiation and photosynthetically active radiation. Earth Syst. Sci. Data 15, 1419–1436. http://dx.doi.org/10.5194/essd-15-1419-2023, URL https://essd.copernicus.org/articles/15/1419/2023/, [dataset].

LI-COR Biosciences, 2021. Eddy covariance processing software. URL https://www.licor.com/EddyPro, [software].

Lompar, M., Lalić, B., Dekić, L., Petrić, M., 2019. Filling gaps in hourly air temperature data using debiased ERA5 data. Atmosphere 10, http://dx.doi.org/10.3390/atmos10010013, URL https://www.mdpi.com/2073-4433/10/1/13.

Machado, R.B., Ramos Neto, M.B., Pereira, P.G.P., Caldas, E.F., Gonçalves, D.A., Santos, N.S., Tabor, K., Steininger, M., 2004. Estimativas de perda da área do Cerrado brasileiro Sugestão de citação. URL http://jbb.ibict.br//handle/1/357.

Mahecha, M.D., Reichstein, M., Carvalhais, N., Lasslop, G., Lange, H., Seneviratne, S.I., Vargas, R., Ammann, C., Arain, M.A., Cescatti, A., Janssens, I.A., Migliavacca, M., Montagnani, L., Richardson, A.D., 2010. Global convergence in the temperature sensitivity of respiration at ecosystem level. Science 329, 838–840. http://dx.doi.org/10.1126/science.1189587, URL https://www.science.org/doi/abs/10.1126/science.1189587.

Mauder, M., Foken, T., 2004. Documentation and instruction manual of the eddy covariance software package TK2. Arbeitsergebnisse 26, Universität Bayreuth, Abt. Mikrometeorologie, URL https://epub.uni-bayreuth.de/id/eprint/884/1/ARBERG026.pdf.

Meehl, G.A., Zwiers, F., Evans, J., Knutson, T., Mearns, L., Whetton, P., 2000. Trends in extreme weather and climate events: Issues related to modeling extremes in projections of future climate change. Bull. Am. Meteorol. Soc. 81, 427–436. http://dx.doi.org/10.1175/1520-0477(2000)081<0427:TIEWAC>2.3.CO;2, URL https://journals.ametsoc.org/view/journals/bams/81/3/1520-0477_2000_081_0427_tiewac_2_3_co_2.xml.

Michaelis, L., Menten, M.L., 1913. Die kinetik der invertinwirkung. Biochem. Z. 49, 333–369, published online in 2007. URL https://publikationen.ub.uni-frankfurt.de/frontdoor/index/index/docId/17273.

Miranda, A., Miranda, H., Grace, J., Meir, P., Lloyd, J., 1996. Carbon dioxide fluxes over cerrado sensu stricto, Central Brazil. In: Amazonian Deforestation and Climate. John Wiley & Sons Inc., United States, pp. 353–364.

Miranda, A.C., Miranda, H.S., Lloyd, J., Grace, J., Francey, R.J., McIntyre, J.A., Meir, P., Riggan, P., Lockwood, R., Brass, J., 1997. Fluxes of carbon, water and energy over Brazilian cerrado: an analysis using eddy covariance and stable isotopes. Plant, Cell & Environ. 20 (3), 315–328. http://dx.doi.org/10.1046/j.1365-3040.1997.d01-80.x, URL https://onlinelibrary.wiley.com/doi/abs/10.1046/j.1365-3040.1997.d01-80.x.

Moncrieff, J., Clement, R., Finnigan, J., Meyers, T., 2005. Averaging, detrending, and filtering of eddy covariance time series. In: Handbook of Micrometeorology: A Guide for Surface Flux Measurement and Analysis. Springer Netherlands, Dordrecht, pp. 7–31. http://dx.doi.org/10.1007/1-4020-2265-4_2.

Moncrieff, J.B., Massheder, J.M., de Bruin, H., Elbers, J., Friborg, T., Heusinkveld, B., Kabat, P., Scott, S., Soegaard, H., Verhoef, A., 1997. A system to measure surface fluxes of momentum, sensible heat, water vapour and carbon dioxide. J. Hydrol. 188–189, 589–611. http://dx.doi.org/10.1016/S0022-1694(96)03194-0, URL https://www.sciencedirect.com/science/article/pii/S0022169496031940.

Montgomery, R.B., 1947. Viscosity and thermal conductivity of air and diffusivity of water vapor in air. J. Meteorol. 4, 193–196. http://dx.doi.org/10.1175/1520-0469(1947)004<0193:VATCOA>2.0.CO;2.

Moore, C.J., 1986. Frequency response corrections for eddy correlation systems. Bound.-Layer Meteorol. 37, 17–35. http://dx.doi.org/10.1007/BF00122754.

Muñoz Sabater, J., 2019. ERA5-land monthly averaged data from 1950 to present. http://dx.doi.org/10.24381/cds.68d2bb30, URL https://cds.climate.copernicus.eu/cdsapp#!/dataset/10.24381/cds.68d2bb30?tab=overview, [dataset].

Nasrullah, Ali, S., Umar, M., Sun, L., Naeem, M., Yasmin, H., Khan, N., 2022. Flooding tolerance in plants: from physiological and molecular perspectives. Braz. J. Bot. 45, 1161–1176. http://dx.doi.org/10.1007/s40415-022-00841-0.

Olson, D.M., Dinerstein, E., Wikramanayake, E.D., Burgess, N.D., Powell, G.V.N., Underwood, E.C., D'amico, J.A., Itoua, I., Strand, H.E., Morrison, J.C., Loucks, C.J., Allnutt, T.F., Ricketts, T.H., Kura, Y., Lamoreux, J.F., Wettengel, W.W., Hedao, P., Kassem, K.R., 2001. Terrestrial Ecoregions of the World: A New Map of Life on Earth: A new global map of terrestrial ecoregions provides an innovative tool for conserving biodiversity. BioScience 51 (11), 933–938. http://dx.doi.org/10.1641/0006-3568(2001)051[0933:TEOTWA]2.0.CO;2.

Pennypacker, S., Baldocchi, D., 2016. Seeing the fields and forests: Application of surface-layer theory and flux-tower data to calculating vegetation canopy height. Bound.-Layer Meteorol. 158, 165–182. http://dx.doi.org/10.1007/s10546-015-0090-0.

Platter, A., Scholz, K., Hammerle, A., Rotach, M.W., Wohlfahrt, G., 2024. Agreement of multiple night- and daytime filtering approaches of eddy covariance-derived net ecosystem CO2 exchange over a mountain forest. Agricult. Forest. Meterol. 356, 110173. http://dx.doi.org/10.1016/j.agrformet.2024.110173, URL https://www.sciencedirect.com/science/article/pii/S0168192324002867.

Ratter, J.A., Ribeiro, J.F., Bridgewater, S., 1997. The Brazilian cerrado vegetation and threats to its biodiversity. Ann. Botany 80 (3), 223–230. http://dx.doi.org/10.1006/anbo.1997.0469, URL https://www.sciencedirect.com/science/article/pii/S0305736497904698.

Roberti, D.R., Mergen, A., Gotuzzo, R.A., Veeck, G.P., Bremm, T., Marin, L., Quadros, F.L.F.d., Jacques, R.J.S., 2024. Sustainability in natural grassland in the Brazilian pampa biome: Livestock production with CO2 absorption. Sustainability 16, 3672. http://dx.doi.org/10.3390/su16093672, URL https://www.mdpi.com/2071-1050/16/9/3672.

Rößger, N., Wille, C., Holl, D., Göckede, M., Kutzbach, L., 2019. Scaling and balancing carbon dioxide fluxes in a heterogeneous tundra ecosystem of the Lena River Delta. Biogeosciences 16, 2591–2615. http://dx.doi.org/10.5194/bg-16-2591-2019, URL https://bg.copernicus.org/articles/16/2591/2019/.

Runkle, B.R.K., Sachs, T., Wille, C., Pfeiffer, E.-M., Kutzbach, L., 2013. Bulk partitioning the growing season net ecosystem exchange of CO 2 in Siberian tundra reveals the seasonality of it carbon sequestration strength. Biogeosciences 10, 1337–1349. http://dx.doi.org/10.5194/bg-10-1337-2013, URL https://bg.copernicus.org/articles/10/1337/2013/.

Sanchez, P., 1979. Pasture production in acid soils of the tropics. In: Series 03 EG / Centre Internacional De Agricultura Tropical, CIAT, URL https://books.google.de/books?id=XgyrUcULGZgC.

Santana, D.P., Bahia Filho, A.F.C., 1998. Soil quality and agricultural sustainability in the Brazilian Cerrado. URL http://www.alice.cnptia.embrapa.br/alice/handle/doc/482346.

Santos, A.J.B., Quesada, C.A., Da Silva, G.T., Maia, J.F., Miranda, H.S., Miranda, A.C., Lloyd, J., 2004. High rates of net ecosystem carbon assimilation by Brachiara pasture in the Brazilian Cerrado. Global Change Biol. 10 (5), 877–885. http://dx.doi.org/10.1111/j.1529-8817.2003.00777.x, URL https://onlinelibrary.wiley.com/doi/abs/10.1111/j.1529-8817.2003.00777.x.

Santos, A.J.B., Silva, G.T.D.A., Miranda, H.S., Miranda, A.C., Lloyd, J., 2003. Effects of fire on surface carbon, energy and water vapour fluxes over campo sujo savanna in central Brazil. Funct. Ecol. 17 (6), 711–719. http://dx.doi.org/10.1111/j.1365-2435.2003.00790.x, URL https://besjournals.onlinelibrary.wiley.com/doi/abs/10.1111/j.1365-2435.2003.00790.x.

Schipper, L.A., Petrie, O.J., O'Neill, T.A., Mudge, P.L., Liáng, L.L., Robinson, J.M., Arcus, V.L., 2019. Shifts in temperature response of soil respiration between adjacent irrigated and non-irrigated grazed pastures. Agric. Ecosyst. Environ. 285, 106620. http://dx.doi.org/10.1016/j.agee.2019.106620, URL https://www.sciencedirect.com/science/article/pii/S0167880919302361.

Schotanus, P., Nieuwstadt, F.T.M., De Bruin, H.A.R., 1983. Temperature measurement with a sonic anemometer and its application to heat and moisture fluxes. Bound.-Layer Meteorol. 26, 81–93. http://dx.doi.org/10.1007/BF00164332.

Seabold, S., Perktold, J., 2010. Statsmodels: Econometric and statistical modeling with python. In: van der Walt, S., Millman, J. (Eds.), Proceedings of the 9th Python in Science Conference. pp. 92–96. http://dx.doi.org/10.25080/Majora-92bf1922-011, [software].

Shapland, T.M., Snyder, R.L., Paw U, K.T., McElrone, A.J., 2014. Thermocouple frequency response compensation leads to convergence of the surface renewal alpha calibration. Agricult. Forest. Meterol. 189–190, 36–47. http://dx.doi.org/10.1016/j.agrformet.2014.01.008, URL https://www.sciencedirect.com/science/article/pii/S0168192314000094.

Silva, J.F., Fariñas, M.R., Felfili, J.M., Klink, C.A., 2006. Spatial heterogeneity, land use and conservation in the cerrado region of Brazil. J. Biogeogr. 33 (3), 536–548. http://dx.doi.org/10.1111/j.1365-2699.2005.01422.x, URL https://onlinelibrary.wiley.com/doi/abs/10.1111/j.1365-2699.2005.01422.x.

Souza, C.M., Shimbo, J.Z., Rosa, M.R., Parente, L.L., Alencar, A.A., Rudorff, B.F.T., Hasenack, H., Matsumoto, M., Ferreira, L.G., Souza-Filho, P.W.M., de Oliveira, S.W., Rocha, W.F., Fonseca, A.V., Marques, C.B., Diniz, C.G., Costa, D., Monteiro, D., Rosa, E.R., Vélez-Martin, E., Weber, E.J., Lenti, F.E.B., Paternost, F.F., Pareyn, F.G.C., Siqueira, J.V., Viera, J.L., Neto, L.C.F., Saraiva, M.M., Sales, M.H., Salgado, M.P.G., Vasconcelos, R., Galano, S., Mesquita, V.V., Azevedo, T., 2020. Reconstructing three decades of land use and land cover changes in Brazilian biomes with landsat archive and earth engine. Remote. Sens. 12 (17), http://dx.doi.org/10.3390/rs12172735, URL https://www.mdpi.com/2072-4292/12/17/2735.

Tanner, C.B., Thurteh, W., 1969. Anemoclinometer measurements of Reynolds stress and heat transport in the atmospheric surface layer. URL https://apps.dtic.mil/sti/pdfs/AD0689487.pdf.

U.S. Geological Survey, 2023. Landsat normalized difference vegetation index. URL https://www.usgs.gov/landsat-missions/landsat-normalized-difference-vegetation-index#:~:text=NDVI%20is%20used%20to%20quantify,)%20%2F%20(NIR%20%2B%20R), Accessed: 2023-03.

van 't Hoff, J.H., 1900. Lectures on theoretical and physical chemistry. Nature 62, 245. http://dx.doi.org/10.1038/062245c0, URL https://www.nature.com/articles/062245c0.

Vickers, D., Mahrt, L., 1997. Quality control and flux sampling problems for tower and aircraft data. J. Atmos. Ocean. Technol. 14 (3), 512–526. http://dx.doi.org/10.1175/1520-0426(1997)014<0512:QCAFSP>2.0.CO;2, URL https://journals.ametsoc.org/view/journals/atot/14/3/1520-0426_1997_014_0512_qcafsp_2_0_co_2.xml.

Virtanen, P., Gommers, R., Oliphant, T.E., Haberland, M., Reddy, T., Cournapeau, D., Burovski, E., Peterson, P., Weckesser, W., Bright, J., van der Walt, S.J., Brett, M., Wilson, J., Millman, K.J., Mayorov, N., Nelson, A.R.J., Jones, E., Kern, R., Larson, E., Carey, C.J., Polat, İ., Feng, Y., Moore, E.W., VanderPlas, J., Laxalde, D., Perktold, J., Cimrman, R., Henriksen, I., Quintero, E.A., Harris, C.R., Archibald, A.M., Ribeiro, A.H., Pedregosa, F., van Mulbregt, P., Vijaykumar, A., Bardelli, A.P., Rothberg, A., Hilboll, A., Kloeckner, A., Scopatz, A., Lee, A.,

Rokem, A., Woods, C.N., Fulton, C., Masson, C., Häggström, C., Fitzgerald, C., Nicholson, D.A., Hagen, D.R., Pasechnik, D.V., Olivetti, E., Martin, E., Wieser, E., Silva, F., Lenders, F., Wilhelm, F., Young, G., Price, G.A., Ingold, G.-L., Allen, G.E., Lee, G.R., Audren, H., Probst, I., Dietrich, J.P., Silterra, J., Webber, J.T., Slavič, J., Nothman, J., Buchner, J., Kulick, J., Schönberger, J.L., Cardoso, J.V.M., Reimer, J., Harrington, J., Cano Rodríguez, J.L., Nunez-Iglesias, J., Kuczynski, J., Tritz, K., Thoma, M., Newville, M., Kümmerer, M., Bolingbroke, M., Tartre, M., Pak, M., Smith, N.J., Nowaczyk, N., Shebanov, N., Pavlyk, O., Brodtkorb, P.A., Lee, P., McGibbon, R.T., Feldbauer, R., Lewis, S., Tygier, S., Sievert, S., Vigna, S., Peterson, S., More, S., Pudlik, T., Oshima, T., Pingel, T.J., Robitaille, T.P., Spura, T., Jones, T.R., Cera, T., Leslie, T., Zito, T., Krauss, T., Upadhyay, U., Halchenko, Y.O., Vázquez-Baeza, Y., 2020. SciPy 1.0: fundamental algorithms for scientific computing in Python. Nature Methods 17, 261–272. http://dx.doi.org/10.1038/s41592-019-0686-2.

Vourlitis, G.L., Pinto Jr., O.B., Dalmagro, H.J., Arruda, P.H.Z., Lobo, F.A., Nogueira, J.S., 2022. Net primary production and ecosystem carbon flux of Brazilian tropical savanna ecosystems from eddy covariance and inventory methods. J. Geophys. Res.: Biogeosci. 127 (8), http://dx.doi.org/10.1029/2021JG006780, e2021JG006780, URL https://agupubs.onlinelibrary.wiley.com/doi/abs/10.1029/2021JG006780.

Vourlitis, G.L., Priante Filho, N., Hayashi, M.M.S., Nogueira, J.D.S., Caseiro, F.T., Holanda Campelo Jr., J., 2001. Seasonal variations in the net ecosystem CO2 exchange of a mature amazonian transitional tropical forest (cerradão). Funct. Ecol. 15 (3), 388–395. http://dx.doi.org/10.1046/j.1365-2435.2001.00535.x, URL https://besjournals.onlinelibrary.wiley.com/doi/abs/10.1046/j.1365-2435.2001.00535.x.

Vourlitis, G.L., da Rocha, H.R., 2010. Flux dynamics in the cerrado and cerrado–forest transition of Brazil. In: Ecosystem Function in Savannas. CRC Press, pp. 97–116. http://dx.doi.org/10.1201/b10275-8.

Webb, E.K., Pearman, G.I., Leuning, R., 1980. Correction of flux measurements for density effects due to heat and water vapour transfer. Q. J. R. Meteorol. Soc. 106, 85–100. http://dx.doi.org/10.1002/qj.49710644707.

Zhao, Y., Holl, D., Anache, J.A.A., Wendland, E., 2024. A Python script for partitioning 30-minute Eddy Covariance (EC) Net Ecosystem Exchange (NEE) of CO2 data into Gross Primary Production (GPP) and Total Ecosystem Respiration (TER), for the 'BR-IAB: Instituto Arruda Botelho - Wooded Cerrado and Mixed Agriculture' dataset. http://dx.doi.org/10.5281/zenodo.12528643, [dataset].

Zheng, Y., Zhao, Z., Zhou, J.-J., Zhou, H., 2012. Evaluations of different leaf and canopy photosynthesis models: a case study with black locust (robinia pseudoacacia) plantations on a loess plateau. Pak. J. Bot. 44, 531–539, URL https://www.pakbs.org/pjbot/PDFs/44(2)/10.pdf.